TAMPEREEN TEKNILLINEN YLIOPISTO
TAMPERE UNIVERSITY OF TECHNOLOGY

JARI SUIKKOLA

PRINTED STRETCHABLE INTERCONNECTS FOR WEARABLE HEALTH AND WELLBEING APPLICATIONS

Master of Science Thesis

Examiner: Adj. Prof. Matti Mäntysalo
Examiner and topic approved by the Faculty Council of the Faculty of Computing and Electrical Engineering on 3rd June 2015

ABSTRACT

JARI SUIKKOLA: Printed Stretchable Interconnects for Wearable Health and Wellbeing Applications
Tampere University of Technology
Master of Science Thesis, 59 pages
June 2015
Master's Degree Programme in Electrical Engineering
Major: Wireless Communications
Examiner: Adj. Prof. Matti Mäntysalo

Keywords: screen-printing, printed electronics, stretchable electronics, wearable electronics, strain testing

Wearable electronics applications have started to emerge in the consumer markets over the past few years, and the market forecasts look promising. Especially sports and healthcare industries have shown interest in the field, as wearables present possibilities of measuring one's vital signals such as electrocardiography unobtrusively. To improve the unobtrusiveness of the wearable devices, stretchable electronics materials may be a more attractive choice than conventional rigid materials or even flexible materials. The ability of stretchable electronics substrates to adjust to the curvilinear surface of human skin lessens the user's need to pay attention to the device.

The objective of this thesis is to manufacture stretchable interconnects by screen-printing, and to characterize these interconnects. In this thesis, first the theoretical background is covered. Then the printing process is first evaluated by printing test patterns with different line widths, and the limits of the process are found in this manner. Next, special strain test patterns are printed and their initial electrical properties are measured. After this, the samples are stretched and the resistance is measured in real time. This way, the resistance's proportionality of the strain is characterized for the interconnects. The mechanical properties such as the forces required for the strain and permanent deformations are also measured. Last, a small demonstration of a textile-integrated circuit implemented with stretchable materials is presented.

It was discovered, that with the used materials and the used printing process, line width and gap width of 200 μm can be achieved with optimal printing parameters. However, with arbitrary patterns that have numerous different line widths, the optimizing might prove to be complicated. Hence, to have 95% throughput yield the minimum line width that can be used is 440 μm and the minimum gap width is 390 μm. The resulting sheet resistance for the manufactured strain test patterns had a mean value of 36.3 $m\Omega/\square$. However, the values had significant deviations, and the process should be optimized in the future. In the strain tests, half of the samples lose conductivity at approximately 74.1% strain. The normalized resistances of the samples rise linearly to approximately 30-40% strain, after which the growth rate starts to increase and is no longer linear. It was also discovered that no cracking can be found from the traces under 30% strains. In the mechanical tests, it was discovered that the force required to stretch these interconnects decreases after one strain cycle, and continues to slightly decrease on the following cycles. Due to this, the stretchable interconnects should be prestretched in the future in order to improve the unobtrusiveness of the application.

TIIVISTELMÄ

JARI SUIKKOLA: Painetut venyvät johtimet puettaville urheilu- ja terveydenhuoltosovelluksille
Tampereen teknillinen yliopisto
Diplomityö, 59 sivua
Kesäkuu 2015
Sähkötekniikan koulutusohjelma
Pääaine: Wireless Communications
Tarkastaja: Dos. Matti Mäntysalo

Avainsanat: silkkipaino, painettava elektroniikka, puettava elektroniikka, venyvä elektroniikka

Puettavia elektroniikkasovelluksia on alkanut ilmaantua viime vuosina kuluttajamarkkinoilla, ja markkinaennusteet näyttävät lupaavilta. Erityisesti urheilu- ja terveydenhuoltoalat ovat osoittaneet mielenkiintoaan puettavassa elektroniikassa. Esimerkkinä tästä ovat sovellukset, jotka kykenevät mittaamaan sykettä käyttäjää häiritsemättä. Jotta tätä häiritsemättömyyttä voitaisiin parantaa, venyvät elektroniikkamateriaalit ovat parempi materiaalivalinta, kuin jäykkiin tai taipuisiin materiaaleihin perustuva elektroniikka. Venyvien elektroniikkamateriaalien kyky sopeutua ihmisen ihon monimuotoiseen pintaan vähentää käyttäjän tarvetta kiinnittää huomiota laitteeseen.

Tämän diplomityön tarkoituksena on valmistaa venyviä johtimia silkkipainotekniikalla, ja karakterisoida näin valmistetut johtimet. Ensimmäisenä tässä työssä kartoitetaan tarvittavat teoreettiset taustat. Seuraavaksi painoprosessin rajat arvioidaan tulostamalla testikuvia eri viivanleveyksiä, ja näin löydetään pienimmät mahdolliset viivanleveydet. Sitten painetaan venytystestikuviot, ja näiden lähtökohtaiset sähköiset ominaisuudet mitataan. Tämän jälkeen näitä näytteitä venytetään, ja resistanssi mitataan reaaliaikaisesti. Tällä tapaa resistanssin riippuvuus venymästä saadaan selvitettyä. Myös johtimien mekaaniset ominaisuudet, kuten venytykseen tarvittavat voimat ja pysyvät muodonmuutokset mitataan. Lopuksi tässä diplomityössä esitellään demonstraatio tekstiiliin integroidusta elektroniikkapiiristä, joka on toteutettu käyttäen venyviä johtimia.

Testeissä havaittiin, että käytetyillä materiaalilla ja painoprosessilla, pienin viivan ja aukon leveys mitä voidaan käyttää on 200 μm kun painoparametrit on optimoitu. Mikäli kyseessä on kuvio, jossa on mielivaltainen määrä eri viivanleveyksiä, tällainen optimointi voi osoittautua haastavaksi. Tällaisessa tapauksessa 95 % saannon saavuttamiseksi pienin viivanleveys, jota voidaan käyttää on 440 μm, ja pienin raonleveys jota voidaan käyttää on 390 μm. Venytyskuvionäytteiden sähköiset ominaisuudet mitattiin ennen venytyksiä, ja näiden neliöresistanssien keskiarvo on 36,3 $m\Omega/\square$. Näissä arvoissa havaittiin merkittävää hajontaa, joten prosessia tulisi optimoida. Venytystestien perusteella puolet näytteistä menettää johtavuutensa noin 74,1 % venymässä. Näytteiden normalisoitu resistanssi nousee lineaarisesti noin 30–40% venymään saakka, jonka jälkeen kasvunopeus alkaa nousta ja ei ole enää lineaarista. Testeissä myös havaittiin, että mekaanisia vaurioita, kuten halkeamia, ei ole havaittavissa alle 30 % venymillä. Mekaanisissa testeissä havaittiin, että johteiden venyttämiseen tarvittava voima vähenee jokaisella venytyssyklillä. Tästä johtuen johtimien esivenyttämistä tulisi kokeilla tulevaisuudessa, sillä tämä voi parantaa sovellusten käyttömukavuutta.

PREFACE

This Master's thesis was done at Department of Electronics and Communications Engineering at Tampere University of Technology during 2015. Work was carried out as a part of Wearable Wellbeing –project, which is a project funded by Technology Industries of Finland Centennial Foundation (Teknologiateollisuuden 100-vuotissäätiö).

I would like to thank my thesis examiner Adj. Professor Matti Mäntysalo for guidance and valuable feedback. I would also like to thank everyone in the TUT Laboratory for Future Electronics, especially D.Sc. Juha Niittynen and M.Sc. Tiina Vuorinen, for valuable guidance during this work. In addition, I would like to thank Timo Kankkunen for printing the samples I used in the strain tests.

In addition, I would like to thank all the personnel in the Department of Electronics and Communications Engineering for this enjoyable working environment.

Lastly, I would like to thank my family and friends for the support during this work and my studies.

Tampere, 20.10.2015

Jari Suikkola

CONTENTS

LIST OF SYMBOLS AND ABBREVIATIONS

ACF	Anisotropic Conductive Film
AD	Anderson-Darlington statistic
AFM	Atomic Force Microscopy
AgNW	Silver Nanowire
BLE	Bluetooth Low Energy
CDF	Cumulative Distribution Function
CI	Confidence Interval
CNT	Carbon Nanotube
CSV	Comma Separated Values.
CuNW	Copper Nanowire
ECG	Electrocardiography
GPIB	General Purpose Interface Bus
GPS	Global Positioning System
HTV	High Temperature Vulcanizing
IoT	Internet of Things
IPA	Isopropyl Alcohol
LSR	Liquid Silicone Rubber
LTV	Low Temperature Vulcanizing
MSDS	Material Safety Datasheet
NFC	Near Field Communication
PCB	Printed Circuit Board
PDMS	Polydimethylsiloxane
PVDF	Polyvinylidene Fluoride
SMD	Surface-mount Device
TPU	Thermoplastic Polyurethane
UTS	Ultimate Tensile Strength
UV	Ultraviolet

1. INTRODUCTION

Numerous applications of wearable electronics have emerged in the consumer market over the past few years. Examples of these applications are smart watches which extend the functionality of the smartphones, and head-mounted displays that provide augmented reality vision to assist the user. Also, the wearables have had an impact in the sports industry, as wrist-worn activity trackers that help the user to measure their physical activities have become popular. In the healthcare industry, the same kind of wearables that are able to measure vital signals such as blood pressure and electrocardiography (ECG) have been under research [1]. These applications have a possibility to revolutionize the healthcare industry, as with these applications the patients can be monitored remotely [2]. This way space in the hospital wards can be used more efficiently. In addition, based on the measured data some diseases could be even diagnosed remotely, or the patients could be invited for an examination based on set alarm limits of various vital signals. Also, the data provided by the remote measurements could be utilized in the field of medical research.

However, wearables have several challenges in their design. One of the key challenges is the unobtrusiveness; the devices should be light to carry and it should not draw too much attention by the user. Due to this, using ultra-thin and ultra-flexible stretchable circuit board materials might be a more attractive choice in the wearable applications than the conventional silicon-based circuit boards. [3] This thesis is a part of Wearable Wellbeing –project, which is funded by the Technology Industries of Finland Centennial Foundation (Teknologiateollisuuden 100-vuotissäätiö). In the project, the main deliverable is a shirt capable of measuring one's bioimpedance and sending it over a Bluetooth link for post-processing. The shirt is a stretchable electronics system, which is implemented with hybrid methodology [4]. This means that the functional modules, such as the Bluetooth-radio and the measurement unit, are implemented on small rigid pieces of circuit board, and these functional modules are connected to each other with stretchable interconnects.

The objective of this thesis is to manufacture these interconnects, and to characterize their electrical and mechanical properties. The stretchable interconnects are manufactured with a screen-printing process. The used ink is a stretchable silver ink, and it is printed on a thermoplastic polyurethane (TPU) substrate. First, the limits of the manufacturing process are evaluated by printing test patterns and reviewing them with an optical microscope and by resistance measurement. Next, strain test patterns are printed, and their initial electrical properties are reviewed. To characterize the electromechanical performance of these interconnects, the samples are uniaxially stretched and their re-

sistance is measured continuously. In this thesis, two different test setups to conduct these strain measurements are designed and experimented. Based on the measurement data gained from these tests, the reproducibility of the manufacturing process is evaluated by statistical analysis. Also, the mechanical properties such as residual permanent deformations and forces required for stretching are measured. Last, a small demonstration of a textile-integrated circuit implemented with stretchable materials is presented.

In Chapter 2 of this thesis, the wearable electronics market, currently available consumer products, and research on the field are covered. In Chapter 3, the basic principles of stretchable electronics are examined. This consists of reviewing the necessary physics of elasticity, principles of manufacturing stretchable electronics systems, and conductor and substrate materials and geometries that are used in the stretchable electronics. In this chapter, also the basic theory of screen-printing is reviewed. In Chapter 4, the experiments done in this thesis are covered, and in Chapter 5 the results corresponding to the experiments are presented.

2. WEARABLE ELECTRONICS

Wearable electronics is a term that is used to describe electrical devices that can be worn by the user. For example, battery powered wristbands and smartwatches that are equipped with sensors and wireless communication technologies have emerged in the consumer market over the past few years. Smart glasses and other head-mounted wearable devices are also available as well as textile-integrated smart devices. For a wearable electronics device, the typical properties are that it is battery powered, contains one or more sensors and processor units, and it is capable of wireless communications. Each of these properties poses its own challenges for the design of the device.[5] A high energy density is required of the battery, as the physical size of the electronics is desired to be kept at smallest to minimize the obtrusiveness of the device while maintaining the functionalities over an adequate operating time. With sensors, challenges lie in miniaturization and in embedding them in the wearables. For wireless technologies, the challenges lie in maintaining seamless connection between devices. In addition, there are challenges in the industrial design of the products as it is difficult to make them appealing to the customers. There is also a high possibility that privacy issues will arise concerning wearables such as unauthorized use of the data produced by the device. [6]

However, the wearable technology can be seen as one of the enablers in the development towards the Internet of Things (IoT). Wearables can integrate the people to the digital environment. [7] For example, the technicians in a production line can use smart glasses for augmented reality interactive manuals. [6] The forecasts for the evolution of the wearable electronics market are promising. The market shares of different wearables in 2014 and forecasts for the market shares in 2018 are presented in Figure 1.

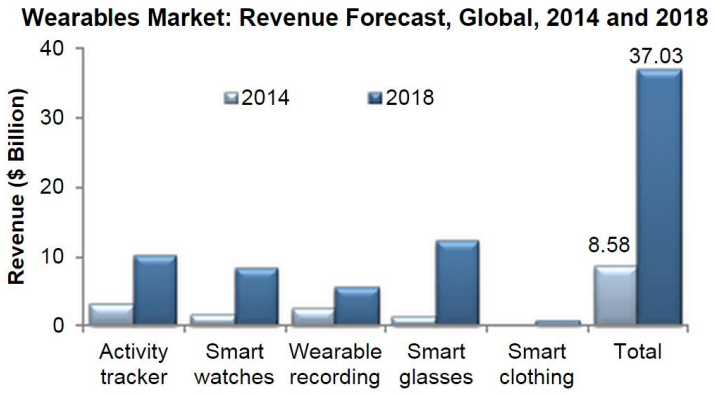

Figure 1. *Wearable electronics market shares in 2014 and forecast for 2018 for different applications.*[6]

An annual growth of 44.1% is expected between the years 2014 and 2018. This would result in revenues of $37.03 billion in 2018. Wearable electronics has also raised interest in the sports industry. One of the first devices in this field is the pedometer, which has been used for decades to measure the step count of the user [8]. Athletes have used heart rate belts together with wrist worn monitoring devices already for years [9]. Recently, wrist-worn activity trackers from companies such as Fitbit, Polar, and PulseOn have become popular. Fitbit Charge HR is presented in Figure 2.

Figure 2. *Fitbit Charge HR is able to measure and show the current heart rate for the user.*

Activity trackers are devices that provide sensor data that is used to quantify the general health and activity of the user. The most of these devices use accelerometers to measure the active minutes and the step count of the user and then provide this data to the user via either the display or Bluetooth connection between the tracker and a smartphone. More advanced models may even be capable of measuring the heart rate of the user and measuring walking distances with Global Positioning System (GPS). The measurement of the same and other health quantifying factors can be also utilized in the healthcare industry. Measurements of different vital signs such as blood pressure and ECG can be done wirelessly without the requirement of physically visiting the hospital [1]. This information can be used for diagnosing diseases in their early stages or it can be used for monitoring patients with chronic diseases. [2] Additionally, the vast amounts of data the remote patient monitoring produces can be utilized in the medical research.

There are also various different kinds of wearables under development with purpose of measuring different health quantifying factors. One of the design goals for these weara-

bles is unobtrusiveness [2]. For example, plasters capable of measuring blood pressure and communicating over near field communication (NFC) have been designed. The components are on a thin and stretchable substrate that can be attached on top of human skin. [10] In addition, a shirt capable of measuring ECG has been studied. The conductive traces in the shirt have been implemented in this study using silver woven fabric [11].

In this thesis, the manufacturing process and the characterization of the stretchable interconnects are done for a project, where the deliverable is a shirt capable of bioelectrical impedance measurement. The shirt is a textile-integrated hybrid system consisting of rigid modules with stretchable interconnects between them. The rigid modules are a power module that uses a coin-cell battery, a Bluetooth low energy (BLE) radio module, and an ECG measurement module. The electrodes are made of the same stretchable materials as the interconnects between the rigid modules. The purpose of this shirt is to measure bioimpedance from the chest of the user and to send this data to a smartphone for post processing. However, the manufacturing of the shirt itself is not in the scope of this thesis, but the target application sets requirements for the stretchable interconnects. These requirements include the durability requirements, biocompatibility requirements, and the possibility of textile-integration.

3. STRETCHABLE ELECTRONICS

In wearable electronics, one of the key design challenges is to make the devices unobtrusive for the user. To succeed in this, the usage of stretchable circuits can be a more suitable choice than the conventional rigid circuit boards or flexible circuits. In stretchable electronics, the wirings are made on thin, ultra-flexible and stretchable substrates. An example of such electronics is presented in Figure 3. In addition, for the circuit to be stretchable, the wirings need to be stretchable as well. An example of the stretchable wirings that are printed on a stretchable TPU substrate is presented on Figure 3.

Figure 3. *Conductive traces printed on a stretchable substrate.*

For example, in epidermal electronics (applications that are affixed to the skin), the devices need to be as lightweight as possible, and they need to be able to adjust to the curvilinear surface of the human skin. This way the user can use the device comfortably without paying any attention to the device. In textile-integrated applications, the comfortability is also an issue. These applications need to be lightweight, and depending on where on the garment the electronics are located, the wirings need to be stretchable. It is estimated that strains of 15-20% occur in the textile throughout the life cycle of the garment [12]. Most of these strains happen when the garment is dressed and undressed. In order to make the textile-integrated electronics comfortable for the user, the circuits need to be able to stretch this much as well, while still maintaining their functionality after the stretching. Based on these estimations, in this thesis the target strain that the interconnects should endure while maintaining conductivity is 30%.

One way of implementing a stretchable electronics circuit is by first miniaturizing each functional module to a small island of rigid circuit board, such as FR4. Then these islands are linked (e.g. glued) to the stretchable printed circuit board (PCB), and the connections between the islands are done by using stretchable interconnects. Together these combinations form a stretchable circuit. Illustration of this principle is presented in Figure 4. [4, p. 145]

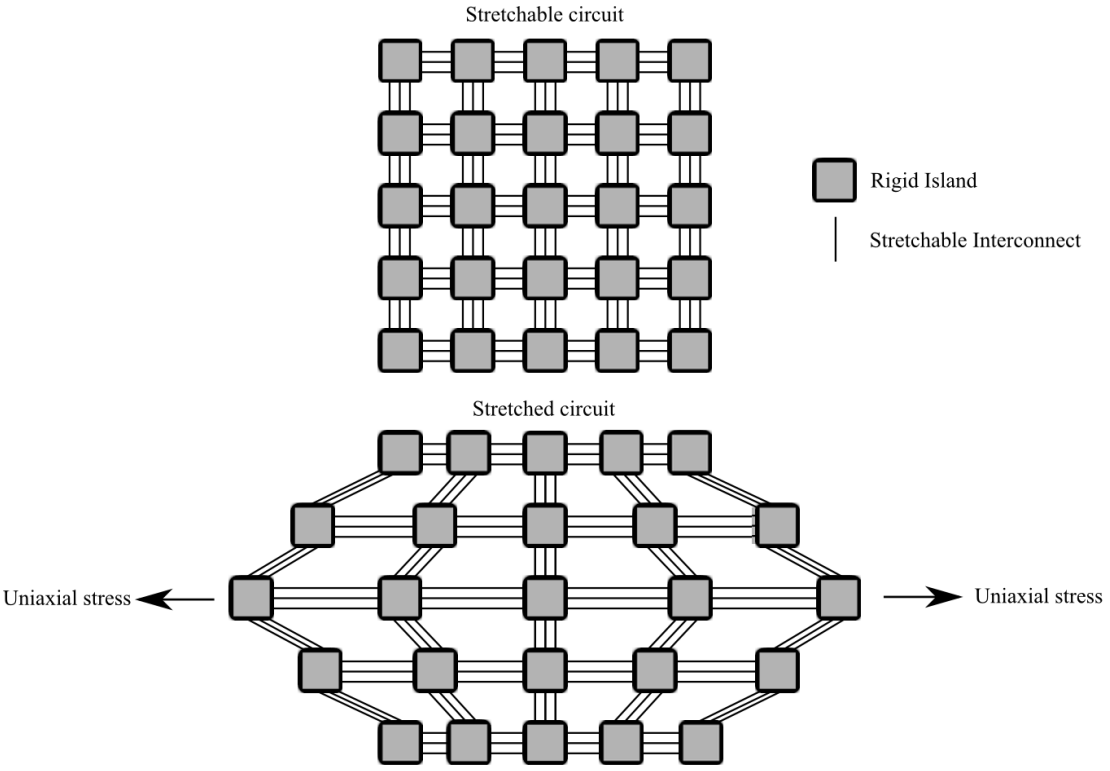

Figure 4. *A hybrid circuit consisting of rigid islands and stretchable interconnects.*

Traditional silicon based devices, such as transistors, can be utilized in manufacturing stretchable circuits by using this type of hybrid principle. Instead of these conventional devices, organic electronics may also be utilized in stretchable circuit manufacturing. Organic devices tend to be more mechanically flexible than their silicon based counterparts, and hence they may be a desirable choice in manufacturing stretchable electronics. However, as of now the performance of the organic devices is poor in comparison, so the applications they can be used in are limited initially. [13] The hybrid circuit methodology is used also in the designing and the manufacturing of the shirt that is discussed in this thesis.

3.1 Mechanical Properties of Stretchable materials

In designing stretchable electronics, it is important to understand the mechanical behavior of the stretchable interconnects. For example in textile-integrated applications, it is important that the forces required for the stretching are not too high, as the unobtrusive-

ness and comfortability of the wearable garment would suffer. In order to comprehend and characterize further the performance of the stretchable interconnects, the essential physics behind elasticity need to be understood.

When an elastic material is loaded, it will deform in relation to the force, and when the load is removed, the material will return to its original state. Hooke's law describes linear elasticity by

$$\sigma = \epsilon E. \tag{1}$$

Here tensile stress σ describes the force per surface area, ϵ is the strain, and E is the Young's modulus or modulus of elasticity. Young's modulus is a constant that is used to characterize the linear elasticity of the material under examination. The tensile stress is calculated as

$$\sigma = \frac{F}{A}. \tag{2}$$

This is the stress required to cause certain strain ϵ for the specimen. The strain ϵ is calculated by

$$\epsilon = \frac{L - L_0}{L_0} \tag{3}$$

Where L is the stretched length of the specimen, and L_0 is the initial length of the specimen. Hence ϵ describes the deformation as a normalized value. It can be also presented as a percentage value. [14]

Another important measure to characterize the stretching of a material is the Poisson's ratio. It represents how much the transverse section of the material deforms in relation to the axial deformation, when axial stress is applied to the specimen. The Poisson's ratio is defined as

$$\nu = -\frac{\epsilon_{trans}}{\epsilon_{axial}}. \tag{4}$$

Here ϵ_{trans} is the transverse strain, and ϵ_{axial} is the axial strain. If the transverse strain is a positive number, it means that the specimen has compressed. In the case of negative number, the specimen has stretched in that direction. For the axial strain, the negative number means that the specimen is compressed in that direction, and the positive number means that the specimen is stretched in that direction.

In characterizing the elasticity of a material, stress-strain curves are a commonly used tool in engineering. The stress-strain curve of an arbitrary material is presented in Figure 5.

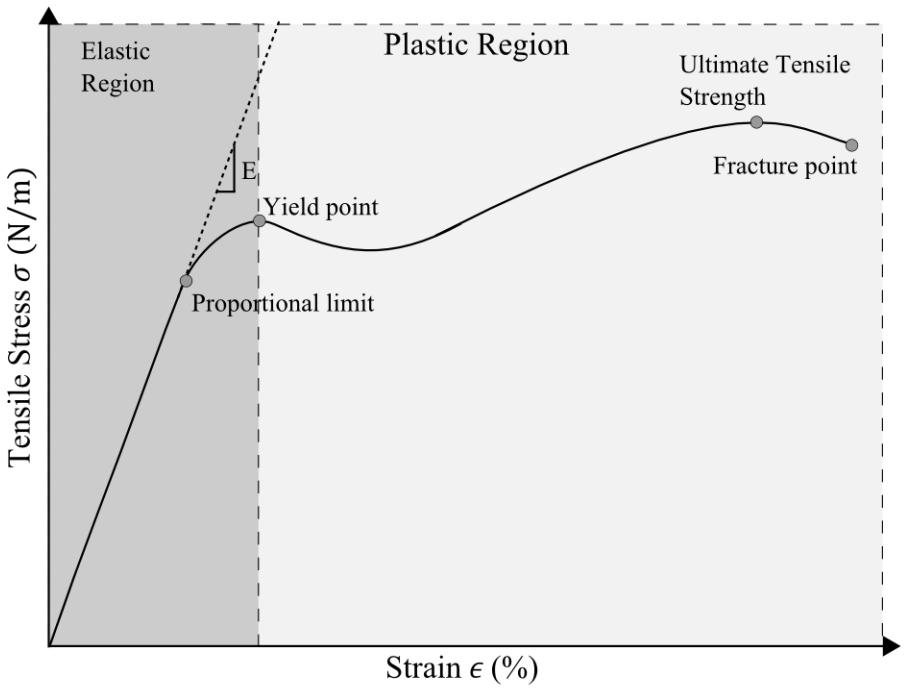

Figure 5. *An example stress-strain curve of an arbitrary material.*[15]

In the stress-strain curve, the stretching can be divided into elastic and plastic regions. In the elastic region, the material will not undergo any permanent deformations, and it is linear and acts according to Hooke's law until the proportional limit. After the proportional limit is reached, Hooke's law is no longer obeyed and the stress-strain performance is nonlinear. When the yield point is reached, the elastic region ends and begins the plastic region. In the plastic region, the molecular structure of the material will start to rearrange, and the specimen will start to deform permanently. Due to this structural reformation, the stress begins to decrease for a while with the increased strain, and then the stress starts to increase again until the ultimate tensile strength (UTS) is reached. From this point onward, the strain again softens until the point of fracture. [16]

However, it is important to note, that the example of the stress-strain curve presented in Figure 5 is only for one arbitrary material. These curves vary a lot between different types of materials. For example, metals and elastomers have significantly divergent stress-strain curves.

3.2 Stretchable Substrates

Using stretchable substrates as circuit board material poses new challenges in the manufacturing processes. It would be convenient, if existing microfabrication processes could be utilized in the manufacturing of stretchable electronics. This sets requirements for example for the operational temperatures, chemical inertness, and mechanical proper-

ties. Typical requirements for all stretchable electronics substrates are conformability and high electrical resistance. However, depending on the application of the stretchable electronics, it may need to possess additional attributes. For example, in epidermal applications or clothing-integrated applications, the substrates need to be biocompatible; they cannot cause any harmful effects to the user. [4 p. 82-83]

Elastomers are a common choice for a substrate in the stretchable electronics. They possess low Young's modulus and can exhibit high strains without fracture. In addition, in most cases they can exhibit these high strains without undergoing any permanent deformations. Typical elastomers that are used in stretchable electronics are silicones, polyurethanes, polyvinylidene fluoride (PVDF), and acrylics. [4, p.83]

One of the most commonly used substrates is the silicone rubber, polydimethylsiloxane (PDMS). PDMS substrates can be roughly divided into three subcategories, depending on which curing conditions and manufacturing processes have been used. These are the high temperature vulcanizing –types (HTV), liquid silicone rubber -types (LSR), and low temperature vulcanizing -types (LTV). Each of these types have slightly different mechanical properties, such as hardness, ultimate tensile strength, and fracture points. However, common properties for PDMS substrates are that each of them exhibit chemical inertness, highly constant mechanical properties over wide operation temperature range, high biocompatibility, and highly elastic behavior. Yet using PDMS can be challenging especially in the printed applications due to its low surface energy, which may result in adhesion problems unless additional surface treatment processes are used.[4, p. 161-171]

Polyurethanes are widely used and studied polymers. There are various different types of polymers ranging from soft to rigid materials. Polyurethanes are highly elastic materials; they may exhibit strains up to 1000%. However, typical maximum strains are in the order of 200%. Between different types of polyurethanes, the hardness may vary a lot, and most of them have high abrasion resistance and are chemically resistant. In this thesis, TPU is used as the substrate. TPUs are highly elastic, and they may show UTS up to 60 MPa and their hardnesses vary from 65 Shore A to 50 Shore D. Typical upper temperature limit of TPU is at around 120 °C. However, at higher temperatures, TPU can be shaped to desired form and then cooled again, and it will maintain its new form. The temperature range where this can be done is called the softening range. If higher operating temperatures are needed from the substrate, then cast polyurethanes might be a more suitable option. However, they cannot be reshaped with heat. [4, p. 171-181] The TPU substrate used in this thesis is a commercially available product, Epurex Platilon U 4201. The material characteristics of this product are presented in Table 1.

Table 1. *Material characteristics of Epurex Platilon U 4201.* [17]

Density (g/cm^3)	1.15
Softening range (°C)	155-185
Hardness (Shore A)	87
Stress at break (Mpa)	60
Stress at 50% strain (Mpa)	5-7
Strain at break (%)	550
Thickness (µm)	50

The main reasons for choosing TPU over other stretchable substrates in this thesis are its high surface energy, and its thermoformability. The high surface energy is beneficial for the printing process as it increases the possibility of good adhesion between the ink and the substrate. The thermoformability can be exploited in the textile-integration. Additionally, the high abrasion resistance of the TPU makes the shirt comfortable to wear.

However, using TPU poses its own challenges. The stress-strain behavior of TPU is non-linear and requires further analysis. It exhibits several uncommon behaviors, which are hysteresis, time dependence, and softening. The hysteresis effect occurs over time; when a sample is loaded and then unloaded, some of the strain persists, and this may first appear as permanent deformation. However, this residual strain partly diminishes over time. For example, Qi et al. report in their tests residual strain of 15% to be decreasing to 6.2% one minute after unloading a sample from a strain of 100% [18]. The time dependence –effect consists of two parts. Firstly, the stress-strain behavior is dependent of the stretch rate; the higher the rate, the higher the stress required for strain. Secondly, if the strain is held constant, the stress required to withhold the strain decreases over time. The softening is also known as the Mullins' effect. This effect occurs over a certain amount of load-unload cycles to a certain maximum strain. After each cycle, the stress required decreases. However, this behavior stabilizes after a certain amount of cycles. Also, the shape of the curve is the same with each cycle, but with lower offset of stress. In addition, on the later cycles when the strain approaches the initial maximum strain of the first cycle, the stress approaches the same value as in the first cycle. [18]

3.3 Stretchable Interconnects

In order to make the interconnects stretchable, firstly the substrate needs to be stretchable. Secondly, the wirings must be stretchable as well. Conductive materials that are used in conventional circuit boards, such as copper and silver, do not meet the stretchability requirements for the most of applications in stretchable electronics in their bulk forms. However, instead of bulk metals, composite- and nanomaterials with desired mechanical and electrical properties may be utilized as the conductive material in the

stretchable interconnects. In addition, there are patterning strategies that may either be utilized to enhance the stretchability for intrinsically stretchable conductors or enable the use of conventional bulk metal conductors in stretchable electronics.

3.3.1 Structural Strategies for Enhancing Stretchability

The aforementioned structures can be divided into out-of-plane structures and in-plane structures. In the out-of-plane structures, the buckling effect of the conductor materials is exploited. Illustrations of the out-of-plane structures are presented in Figure 6.

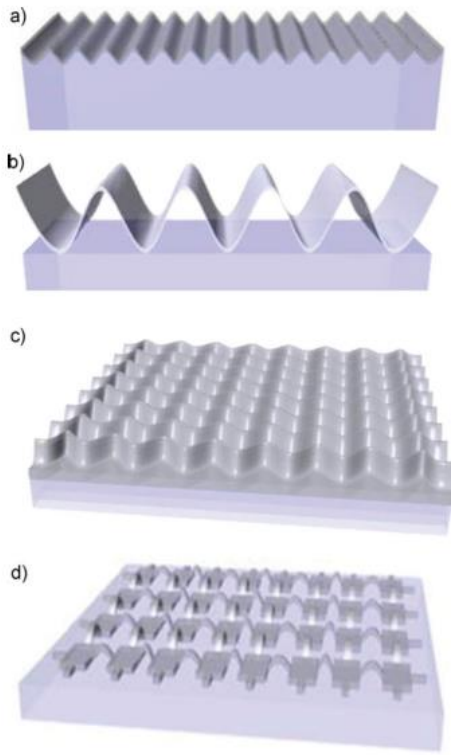

Figure 6. *a) Stretchable wavy ribbons. b) Pop-up structure. c)Two-dimensional wavy membrane. d) Two-dimensional buckled mesh.* [19] *Reprinted with permission from John Wiley and Sons.*

The buckling effect can be applied to the conductor by implementing the following steps in the manufacturing process. Firstly, the stretchable substrate is pre-stretched. Secondly, the conductor is bonded to the substrate. Finally, the stress is released and the substrate compresses to its original form, causing the bonded conductor to buckle. Furthermore, there are several slightly different strategies used in the manufacturing of out-of-plane structures. The structure in Figure 6 a) is called the stretchable wavy ribbons, and in this structure the conductor is bonded to the substrate throughout its whole length. In Figure 6 b) is the pop-up structure, where the conductor is bonded only at certain locations. The advantage of the pop-up structure is that the wavelength of the

buckling may be specified, thus giving more control over the stretchability of the interconnect. The disadvantage is that the substrate provides the mechanical support for the conductor only at the bonded locations, making the conductor structure fragile in comparison to the wavy ribbons. In Figure 6 c) the two-dimensional wavy membrane is introduced. In this structure, the principle of wavy ribbons have been applied to two dimensions. In Figure 6 d) the principle of pop-up structure have been applied to a two-dimensional matrix that consists of rigid islands and stretchable interconnects. In this case, only the rigid islands are bonded to the stretchable substrate. [4][19]

The problem with the out-of-plane structures is that they are difficult to implement in a production line (e.g. roll-to-roll) process. Processwise, a simpler way of manufacturing stretchable interconnects is to use in-plane geometries for the conductor. Examples of this type of structures are presented in Figure 7.

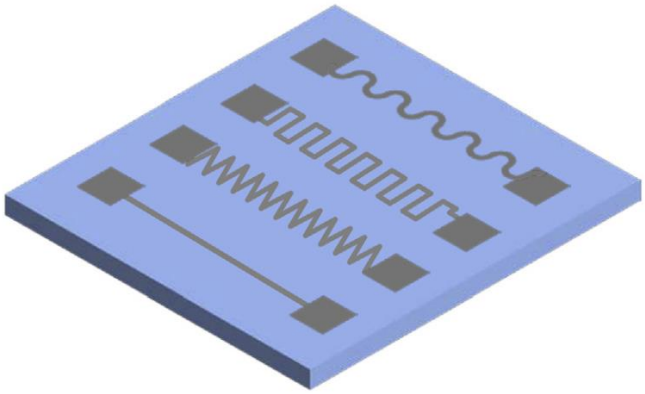

Figure 7. *Single line, zigzag, pulse, and horseshoe geometries.*[20] *Reprinted with permission from Elsevier.*

Single line structure is a commonly used structure in conventional electronics, but in stretchable electronics, this structure may only be used if the conductive material is intrinsically elastic. Zigzag, pulse, and horseshoe geometries allow higher deformations than the single lines. The principle of these structures is similar to a spring; the structure actually bends from certain sections, which results in the stretching of the whole structure. In these structures, especially in the zigzag and pulse geometries, the stress is focused on the corner areas. This makes these areas the most likely locations where the structure is going to break. With the horseshoe geometry, the stress area is wider in comparison to the zigzag and pulse geometries. In the literature, there have been simulations and practical studies that have compared the stretchability of these three geometries, and on several occasions the horseshoe has proven to provide the highest stretchability [4][20]. However, it is important to note that the stretchability of these geometries can be controlled and optimized by alternating the dimensions of the geometries. In addition, there may be differences that appear depending on the manufacturing methods and the material choices.

3.3.2 Advanced Materials for Stretchable Interconnects

The material for stretchable interconnects is required to possess a high electrical conductivity and high mechanical deformability. Depending on the application, it may be only required that the material is conductive on its initial and returned states, or it may be beneficial to maintain the electrical conductivity also during the high strains. One way to enhance the stretchability is using composite materials, where nanomaterials have been combined with elastomeric materials. In this method, the nanomaterials form conductive networks while the elastomeric materials provide the elasticity. However, while the increased amount of the conductive nanomaterials increase the conductivity of the material, at the same time it increases the brittleness and rigidness. Hence, depending on the application, the ratio between the component materials dictates the electromechanical properties of the outcome. In addition, additional surfactants, purity of the nanomaterials, and the chosen dispersion techniques may play key roles for further improving the performance of the composite material. There are several different types of nanomaterials that have been utilized in the fabrication of the stretchable conductor materials. Examples of these nanomaterials are composites made of carbon nanotubes (CNT) and elastomers, conductors based on metal-nanowires such as silver nanowires (AgNW) and copper nanowires (CuNW), and graphene-based solutions. [21]

The material used for fabricating the stretchable interconnects in this thesis is a commercially available screen-printed ink, CI-1036 by ECM. Main reasons for choosing this material are its high conductivity and high flexibility guaranteed by the manufacturer, and that it is commercially available. Another reason is that the curing temperature of the ink is lower than the softening range of the substrate. Additional properties from the datasheet of the ink are presented in Table 2. [22]

Table 2. *Properties of the ECM CI-1036 flexible silver ink.*[22]

Uncured Properties	
Viscosity	10 000 CPS at 25°C
Total Solids Content	66 %
Density	2.08 kg/l
Cured Properties	
Sheet Resistance	< 10mΩ/sq.

The total composition of this ink is unknown. However, the hazardous materials of the ink are reported on the material safety datasheet (MSDS) and these ingredients approximately cover the total weight of the ink. The ingredients are presented on Table 3.

Table 3. *Hazardous ingredients of the ECM CI-1036 flexible silver ink* .[23]

Ingredient	% Weight
2-Butenedioic acid (Z-), polymer with chloroethene and ethenyl acetate	1-5%
Silver Flake	50-60%
Diethylene glycol ethyl ether acetate	30-40%

Based on this information, it can be determined that when the ink is cured, the resulting material is a composite material, where the elastic material is the 2-Butenedioic acid (Z-), polymer with chloroethene and ethenyl acetate and the conductive material is the silver flakes.

3.3.3 Screen-Printing

Several different types of fabrication methods have been studied for the manufacturing of stretchable interconnects. For example, thin films of copper have been laminated to TPU substrate and then etched into desired stretchable in-plane geometry [4]. Inkjet printing has also been studied in the manufacturing of stretchable interconnects [24]. One of the most commonly used fabrication methods is the screen-printing, which is also used in this thesis. The main reason for this choice is that screen-printing is the fabrication method recommended by the ink manufacturer, as with the screen-printing parameters there is a high control over the deposition of the ink.

A screen-printer consists of four crucial elements. First of them being the printing paste which is in this thesis the stretchable ink. The second one is the screen, which is used to define the desired pattern for printing. The third one is the surface the ink is deposited on, which in this thesis is the TPU substrate. The fourth one is the squeegee, which is used to push the ink through the screen on to the substrate. In some printers there is also another squeegee that is used to spread the ink on the screen before it is pushed through the openings. An illustration of the screen-printing process is presented in Figure 8.

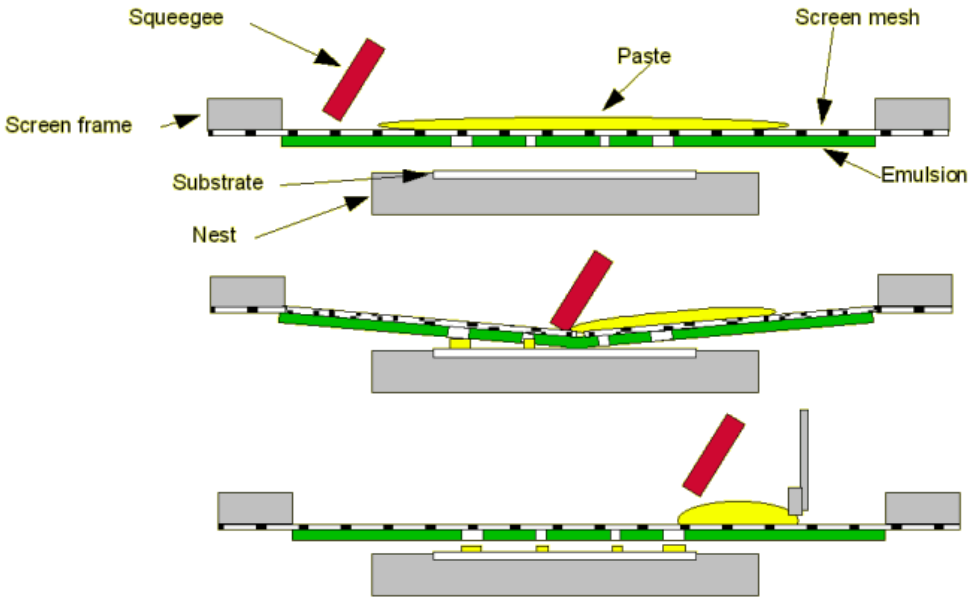

Figure 8. *The principle of the screen-printing process.* [25]

In the beginning of the process, the substrate is under the screen and the ink is deposited evenly on top of the screen. After this, the squeegee is pressed against the screen with such pressure that the screen stretches slightly and at the same time the squeegee moves towards the other end of the screen. Now the squeegee pushes the ink through the screen and the ink is deposited on the substrate, resulting in a pattern defined by the screen. [25]

The screen consists of three different parts; the frame, the mesh and the stencil. The frame is usually made of metal, as it needs to provide sufficient mechanical support for the mesh that is tightly stretched and attached to the frame. The load exerted by the mesh is in the order of 50 kg, so the strength of a metal is required. The most common material used for the mesh in the industry is polyester, but also nylon and stainless steel are used in mesh fabrication. The purpose of the mesh is to provide the mechanical support for the stencil, while still providing the way for the ink to go through it. There are several properties that characterize the mesh; the number of threads per centimeter, thread diameter, mesh opening, open area, cloth thickness, and the screen tension. These properties partly dictate what kind of inks can be used with the screen and what are the properties of the resulting pattern, for example the minimum line width. The mesh opening depends on the particle size of the ink that is desired to be used, and the common rule of thumb for this is that the mesh opening should be at least three times the particle size. The minimum line width depends on the thread diameter, and the common rule of thumb for this is that the minimum line width is three times the mesh thread diameter. However, the manufacturer of the ink commonly provides the recommended parameters of the screen. The purpose of the stencil is to define the desired pattern that is wanted to deposit on the substrate. Additionally, the thickness of the stencil affects the thickness of the printed pattern. One of the most common methods to fabricate the

stencil is by using photo-emulsions. The principle of using photo-emulsions is that first the material is spread on the mesh, then the desired pattern is shadowed using a mask, and the rest of the photo-emulsion is exposed to ultraviolet (UV) light. This way the patterned area remains soluble to warm water, and rest of the emulsion is hardened. When the stencil is now washed, the desired pattern is left open on the stencil and ink can be pushed through the mesh. An example screen that is used to determine the printability of an ink-substrate combination is presented in Figure 9. [25]

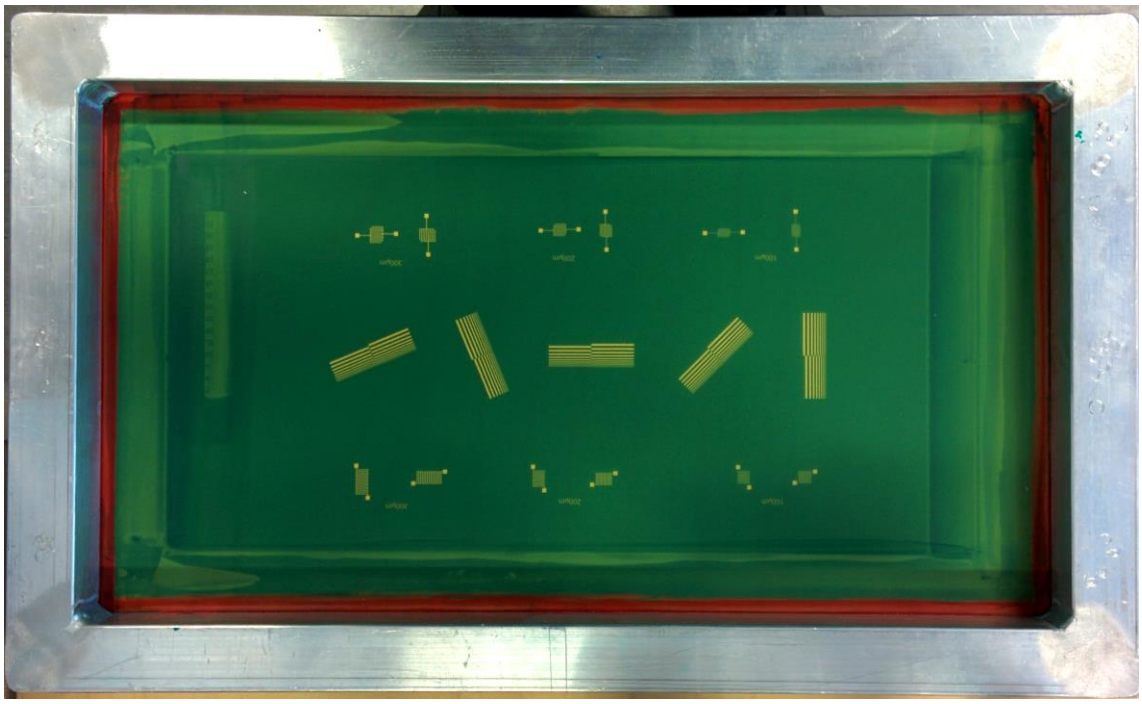

Figure 9. *Top-view image of a screen used in screen-printing.*

In Figure 9, the green area is the emulsion and yellow area is the mesh. The mesh is attached to an aluminum frame.

The squeegee is needed to push the ink through the screen and onto the substrate. The material for the squeegee needs to be solvent resistant. The hardness of the squeegee is also an important parameter. Typical hardness of the squeegee is in the range of 60 to 80 Shore. Soft squeegees accommodate well with irregular surfaces, while harder material with higher squeegee pressures can be used to achieve thinner printed patterns. The shape of the squeegee may also vary, but the square edged shape is the most commonly used. The width of the squeegee should also be wider than the printed pattern by at least 10 mm from both sides, because the screen tension tends to bend the ends of the squeegee. The angle between the screen and the squeegee is also one parameter that can be adjusted, but for the most cases an angle of approximately 45° provides the best result. [25]

As one may notice, there is a myriad of parameters to be considered in the screen-printed in order optimize the quality of the printed pattern. The properties of the squee-

gee such as hardness, dimensions and shape, the properties the ink used such and viscosity and solids content, the properties of the screen such as mesh count and screen tension, the properties of the printing machine such as parameter controls, the properties of the substrate, and the properties of the printing process such as squeegee pressure and print speed all affect the printing quality. Qualifying factors can be for example the mean thickness of the printed line versus the thickness defined by the stencil, thickness uniformity, and fine line resolution. However, once the parameters are optimized, they can be commonly kept constant throughout the printing process.

4. EXPERIMENTS

In this thesis, stretchable interconnects are manufactured and their electrical and mechanical performance is evaluated. In the fabrication process, the printability is first studied. After suitable parameters have been found, test patterns are printed which are used in the strain testing. First the initial sheet resistance is measured from these samples, and then the electrical and mechanical performances are evaluated in the strain tests.

4.1 Screen-Printing Fabrication with Stretchable Materials

In this thesis, the stretchable interconnects are manufactured by screen-printing. The material used as the substrate for the interconnects is Epurex Platilon U4201 TPU. The ink used for printing the conductors is the CI-1036 by ECM.

Two different screens are used in this thesis. Firstly, the limits of the process and the material combination are evaluated by using a screen that is filled with printability test patterns. Secondly, a screen that is used for printing a strain testing pattern is used. The screens were ordered with parameters based on the recommendations of the ink manufacturer and the dimension limits of the screen-printer and the squeegee. The parameters of the screens are presented in Table 4.

Table 4. *Parameters of the screens that are used in this thesis.*

Mesh Material	Polyester
Frame Material	Aluminum
Frame Dimensions (mm^2)	500 x 3000
Frame Profile (mm^2)	30 x 30
Mesh Count (threads/cm)	79
Mesh Opening (µm)	69
Thread Diameter (µm)	55
Theoretical Wet Paste Thickness (µm)	26
Stretching Angle (°)	22.5

The hardness of the rubber squeegee used in this thesis is 75 Shore, as this is recommended by the ink manufacturer. The shape of the squeegee is square-edged.

The manufacturing process is started by cutting the TPU into sheets. After this, the sheets are attached on the surface of aluminum plates. In this process, the substrate is pre-stretched slightly (in the order of 5%) and its edges are attached to the other side of the plate by using the plate with kapton tape. Due to the soft nature of the 50 µm thick TPU substrate, this procedure is necessary to make sure that the substrate stays steadily flat throughout the whole printing process, including the curing. After the TPU is attached to the aluminum plate, its surface is carefully cleaned with isopropyl alcohol (IPA), in order to make sure that there is no stains or dust that could impair the printing quality.

The CI-1036 screen-printed ink is stored in under 15 °C temperature. Before printing, the ink is first prepared for printing by holding it in room temperature for approximately one hour. Additionally, before the printing is started, the ink needs to be gently stirred with a spatula for 1-2 minutes. These pre-conditioning steps are done to make sure that the rheology of the ink is suitable for screen-printing and stays approximately the same throughout the printing process.

The device used is the SCF-300 semi-automatic screen-printer by TIC. The printer is presented in Figure 10.

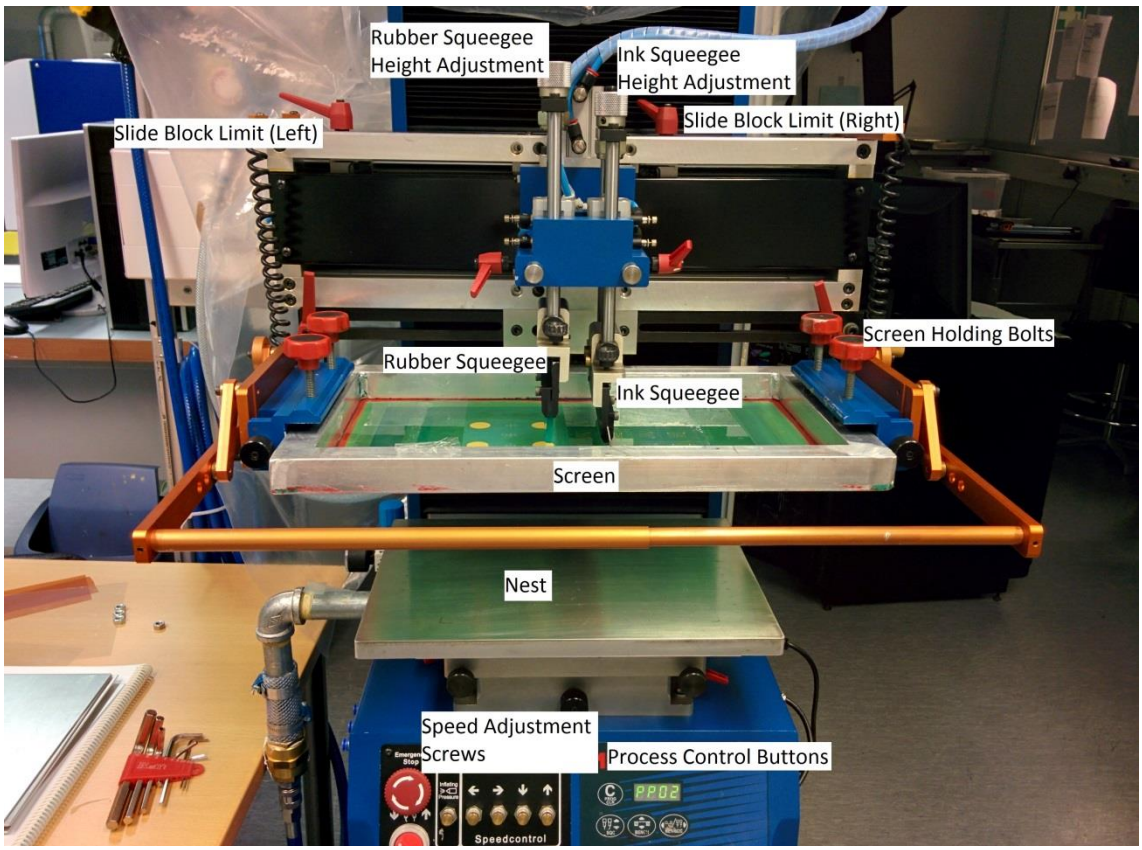

Figure 10. *The screen-printer used in this thesis, TIC SCF-300.* [26]

After the screen and squeegees are installed to the printer, the printing process is started by adjusting the printing length with using the slide block limits. The block limits are adjusted so that the squeegees end up only at the edges of desired pattern in order to minimize the area where the ink is spread. The next step is placing the substrate on the nest of the screen-printer. After this, the screen is lowered on top of the substrate by the process control buttons. Next, the ink is added to the right side of the pattern, which is followed by spreading the ink with the ink squeegee. The height of the ink squeegee is adjusted so that it is barely on top of the screen but not touching it, as the metallic squeegee can damage the polyester screen. However, it should be low enough that it can spread the ink evenly on top of the screen. Commonly a suitable height is approximately 0.5 mm above the screen. The process control buttons are used to move the squeegees. After the ink is spread over the pattern, the ink squeegee is risen up and the rubber squeegee is lowered down. The initial height of the rubber squeegee (i.e. the squeegee pressure) is adjusted so that it slightly presses the screen. The initial pressure is good when some ink barely is transferred to the substrate. After the pressure is adjusted, the rubber squeegee is moved to the right side of the screen by using the process control buttons, and the rubber squeegee pushes ink through the mesh of the screen on the way. After the pattern is deposited to the substrate, the screen stage may be raised and the print quality may be reviewed.

Usually, when printing with this printer, certain parameters need to be readjusted in order to optimize the print quality. The process of optimizing the print quality is presented in Figure 11.

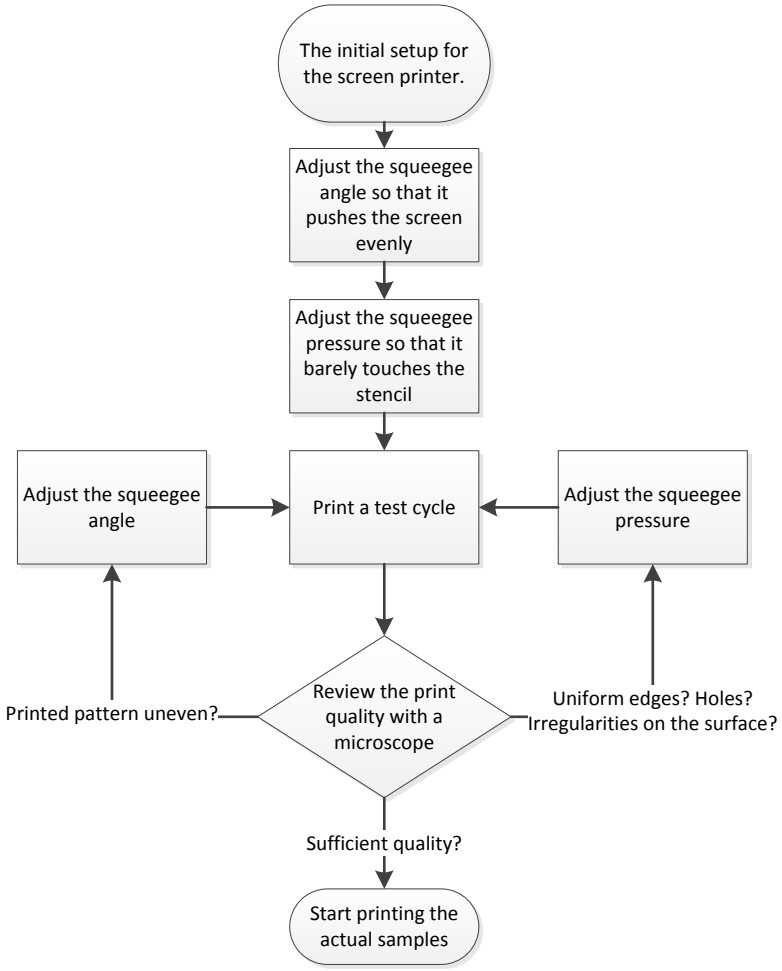

Figure 11. *The process of optimizing the print quality before printing.*

Before printing more samples, first the printing parameters that provide optimal printing quality are searched for. The testing of each combination of printing parameters is done by doing one print on an aluminum plate with no TPU attached to it. This is done because the ink is easily cleaned from the aluminum with acetone. After each test cycle, the print quality is evaluated with an optical microscope. In the microscope review, the things that are checked are the uniformity of the edges of the printed line, and the presence of holes and irregularities. If there are differences between the different ends of the pattern, the parameter that is adjusted is the squeegee angle transverse to its movement direction. If the edge of the printed line is wavy or there are holes or irregularities, the squeegee pressure is readjusted. The optimization process is repeated until the printing quality is sufficient. Another way to improve the print quality and the electrical performance of the pattern is by doing additional cycles of ink spreading and deposition on the same substrate sheet. This way more ink is deposited on the substrate, which may for example fill holes left after the first cycle. However, too many cycles may cause the lines to flood, which may cause short circuits between adjacent lines with a narrow gap between them.

After the desired patterns are printed on the substrate, the patterns need to be cured to make them conductive. According to the datasheet of the ECM CI-1036 ink, suitable curing temperature is 125 °C and curing time is 10 minutes. However, the use of the aluminum plates increases the required curing time. A suitable curing schedule was found with a process where the patterns were in the oven in 10 min cycles and the resistance was measured after each cycle. If the resistance of the patterns had lowered less than 10% between the cycles, no additional cycles are required. The final curing parameters were found to be 125 °C and 30 minutes. After curing, the next step is to cut the substrate around the pattern to a desired shape and then review with optical microscope in order to discover existing faults before further testing.

4.1.1 Fabrication and Review of Printability Test Patterns

In the printability test, several different test patterns are printed. First set of test patterns include line and gap widths from 100 µm to 1000 µm with 50 µm steps in angles of 0°, 22.5°, 45°, 90°, and 112.5°. With these print patterns, the effect of the printing angle is studied as well as the overall printability of narrow lines and gaps. These patterns are presented in Figure 12.

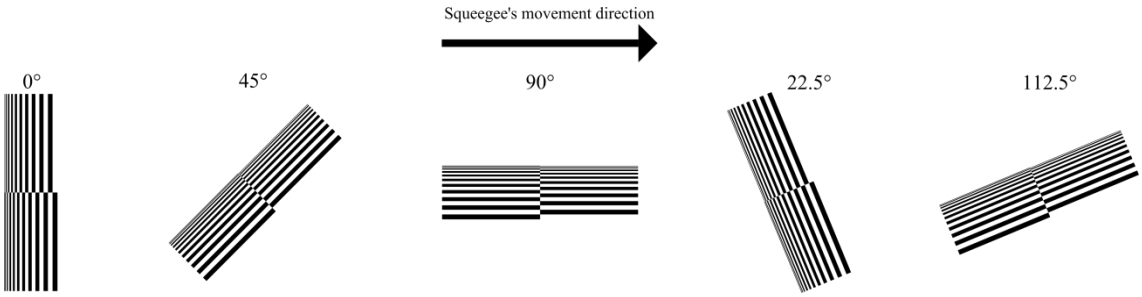

Figure 12. *Printability test patterns in five different angles. Each pattern includes line and gap widths from 100 µm to 1000 µm with 50 µm steps.*

10 samples are manufactured of each of the pattern. These patterns are positioned in this order on the screen, and the squeegee sweeps from left to right. After the fabrication, the samples are reviewed with an optical microscope. On the review, for each sample the narrowest successful line width is sought.

In the another set of test patterns, meander-shaped lines with 200 µm, 300 µm, and 400 µm widths and equal width gaps between them are printed in 0° and 90° angles. Also, capacitor-shapes are printed with same parameters. The meander-shaped patterns are presented in the top row of Figure 13, and the capacitor-shaped patterns are presented in the bottom row of Figure 13.

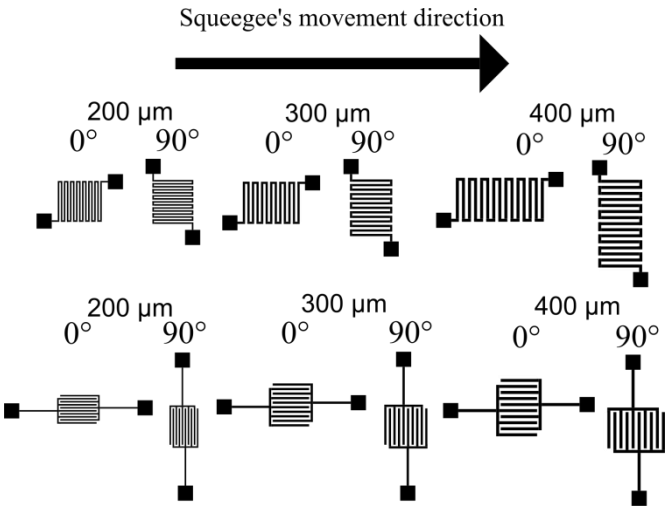

Figure 13. *Printability patterns to further evaluate the line widths and gap widths of 200µm, 300µm, and 400 µm. The meander-shaped test patterns are on the top row, and the capacitor-based patterns are on the bottom row.*

In addition to determining by the microscope review, these patterns are evaluated also by measuring the conductivity between the pads. For the meander-shaped patterns, if there is no conductivity, it can be determined that the lines are cut from somewhere. Also, resistances significantly lower than the average of the lot may indicate overflows that cause shortcircuits between adjacent lines. For the capacitor-shaped patterns, if there is conductivity between the measurement pads, it can be determined that there are overflows that cause shortcircuits between the adjacent lines.

In manufacturing these samples, the TPU is attached to 240 x 240 x 2 mm^3 aluminum plates. The plates of this size are chosen because all of the printability patterns presented are located on one screen, and the patterns are printed with one printing cycle. The printing parameters are optimized for the 200 µm meander-shaped patterns and for the 200 µm capacitor-shaped patterns. After the suitable printing parameters have been found, they are maintained the same and 10 samples of each pattern are printed. These samples were printed by using one ink deposit cycle, and the squeegee pressure is high enough to cause it to bend approximately 45°.

4.1.2 Fabrication of Strain Testing Samples

In addition to printability test patterns, stretchability test samples are also printed in this thesis. The pattern used for strain testing is presented in Figure 14.

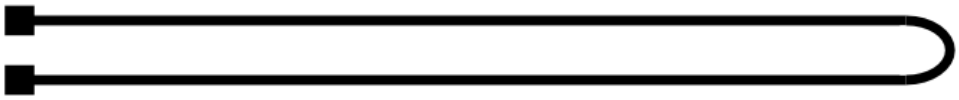

Figure 14. *Strain test pattern. The line width of the trace is 1 mm, and the total length of the trace is 188.9 mm. The pads are 3 x 3 mm^2, and the gap between the traces is 5 mm. The distance between the left and right end of the pattern is 96 mm.*

In the stretchability pattern, 1 mm line width is used. This width is chosen due to the possibility that it will produce higher stretching performance than the thinner lines and because it is still not too wide line width to be used in certain stretchable electronics applications. The total length of the line is 188.9 mm. On the screen, the long traces in the pattern are perpendicular angle towards the squeegee.

In manufacturing these samples, the TPU is attached to 150 x 100 x 2 mm^3 aluminum plates. The plates of this size are chosen because only one sample is printed each time. On every printing time, lots of 10 samples are printed. Three lots are made for the electromechanical tests, and these lots are also examined from the reproducibility point of view. In addition, one lot is printed for the mechanical testing, and one for reviewing the cracking of these samples. All of the samples are printed with approximately the same parameters. These samples are printed by using two ink deposit cycles, and the squeegee pressure is high enough to cause it to bend approximately 45°.

4.2 Sheet Resistance Measurement

In order to characterize the initial electrical properties of the screen-printed ECM CI-1036 ink on the Epurex Platilon U4201 TPU substrate, the resistances of the printed patterns are measured. The resistance R of a three-dimensional line is defined as

$$R = \frac{\rho}{t}\frac{L}{W}. \tag{4}$$

Here ρ is the resistivity of the conductor material, t is the thickness of the conductor, L is the length of the conductor and W is the width of the conductor. For a thin-film application, where commonly the surface roughness is significant in relation to the total thickness of the conductive film, exact thickness may be complex to define. Due to this reason, sheet resistance R_S is commonly used for characterizing the electrical resistivity of the thin-film applications on a general level, rather than resistivity ρ. The unit of the sheet resistance is $[\Omega/\square]$ (ohms per square). The relationship between the sheet resistance and the resistivity is defined

$$R_S = \frac{\rho}{t} \tag{5}$$

Hence, sheet resistance is used to describe the electrical resistivity of a planar structure, without taking the conductor thickness t into account. And as can be seen from (4) and (5), the resistance of a pattern can be calculated by multiplying the sheet resistance with the amount of squares, L/W. Also, when (4) and (5) are combined, it can be noted that the sheet resistance can be calculated as

$$R_S = R\frac{W}{L} \tag{6}$$

when the resistance R of the pattern is measured. Typically, a special pattern such as Greek cross is used to determine the sheet resistance reached by the manufacturing method. [27] These type of special patterns are commonly used because with them 4-point resistance measurement setup can be used. However, in this thesis the sheet resistances are measured using 2-point measurements with the strain testing patterns. As the width W of the strain testing pattern is 1 mm, and length L = 188.9 mm, the sheet resistance is calculated as

$$R_S = \frac{R}{188.9}\ [\Omega/\square] \tag{7}$$

However, it is important to note that this is valid for the desired pattern. In the fabricated samples, the width of the pattern is not constant and the lines are not uniform. In this thesis, the narrowest section measured is 920 µm, and the widest section measured is 1080 µm. This causes an absolute maximum error of 8% for the sheet resistances. However, the error is significantly smaller, as these values are only the narrowest and widest sections of all the samples, and not the mean values of the trace width.

In this thesis, the resistances of all the strain testing samples that have been manufactured for different tests has been measured using the Keithley 2425 Sourcemeter with 2 measurement points. Based on these measurements, the initial conductivity of the ECM CI-1036 on Epurex Platilon U4201 TPU substrate is characterized. Also, the sheet resistances are used to evaluate the reproducibility of the screen-printing process with these materials.

Due to the 2-point measurement, the contact resistances are present in the measurements and need to be reduced. The contact resistances are 1.3 Ω on average, and may deviate between values 1.0 Ω and 1.6 Ω. When the total resistance of the measured pattern and the contacts is in the order of 8 Ω, this causes approximately 4.5% error for the sheet resistance values.

4.3 Electromechanical Test Setups

One way of evaluating the performance of a stretchable interconnect is to measure the change of the electrical resistance when it is being deformed. The simplest and the most common way to do this is to stretch the interconnect uniaxially, and to measure the re-

sistance in real time during the strain testing. In this thesis, two different approaches of this type of test setup are implemented, tested, and evaluated.

4.3.1 Instron 4411 –based Test Setup

The first setup is based on Instron 4411 Universal Testing System that is commonly used for measuring the mechanical properties of materials. This system provides the strain testing functionality, such as strain control and load measurement for the testing, but lacks the resistance measurement. For the resistance measurement purpose, Keithley 2425 sourcemeter is used together with a logger software running on a laptop. The setup is presented in Figure 15.

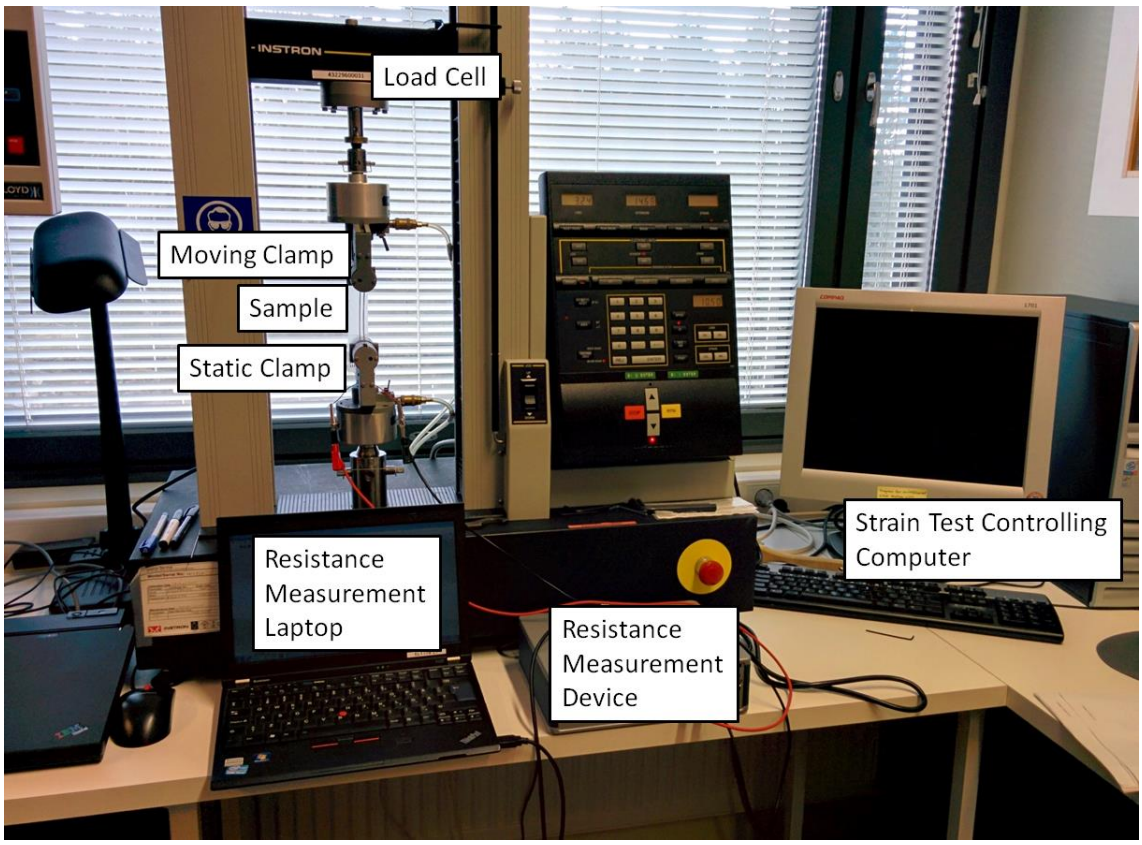

Figure 15. *Instron 4411 Universal Testing System –based test setup.*

In this system, the ends of the measured samples are attached between the two clamps. The other end is static, and the other one moves. The geometry of the strain testing pattern is presented in Figure 14. By choosing this type of curved pattern, both resistance measurement wires can be attached to the static clamp. This way, the possible measurement noise that is caused by attaching a measurement wire to the moving clamp is avoided.

In this setup, the testing is started by first choosing a suitable load cell. In the tests of this thesis, a 500 N load cell is used. After the load cell is attached, the metallic grips

are attached to the cell and to the bottom of the test system. Then, suitable clamps are attached to these grips. In these tests, metallic clamps with pressing area of 38 x 25 mm^2 are used. The pressing areas of these clamps are covered with 1 mm thick rubber pads. After the clamps are attached, the grip distance, i.e. the distance between the clamps are adjusted to a suitable distance. When this initial setup is done, the testing system needs to be calibrated. In the calibration process, the forces caused by the weight of the attachment pieces are reduced from the measurement and the system is presented what load cell is used. After the calibration is done, the measured specimen can be attached to the test setup. The clamps are closed pneumatically and this is controlled by a foot switch. The strain testing itself is controlled by a computer, with software Series IX. In the software, first the dimensions of the measured sample need to be set. This covers the width of the sample, the grip distance used, and the thickness of the sample. This data is used in the software to calculate different mechanical parameters, such as the stress. After the sample dimensions are set, the direction and speed of the clamp movement is specified. Next, the limits of the test are specified. This includes the maximum strain and the maximum load after which the test should stop. The maximum strain should be chosen according to the test plan, and the maximum load should be a bit lower than the maximum load of the load cell. In the tests of this thesis, a maximum load of 0.48 kN is chosen. Finally, the sample rate is chosen. In order to synchronize the load and strain data provided by the Instron system and the resistance data provided by the Keithley 2425 Sourcemeter easy, the sample rates for both devices should be the same. After the sample rate is specified for the Series IX software, the strain test part of the measurement setup is ready for testing. In the testing process, the software logs the strain and load data, and it can be set to retrieve certain mechanical properties, such as Young's modulus, based on the measured data. In the end of the test process, the data is saved as a comma separated values -file (CSV).

In the resistance measurement part, the pads of the measured sample are connected to the resistance measurement ports of the Keithley 2425 sourcemeter. A simple resistance logger software written in LabVIEW programming language controls the measurement process. In the program, the only setup required is setting the correct USB-device, and the correct sample rate. After these are set, the resistance measurement setup is ready for the measurement. In the measurement process, the software records the resistance data and stores this in a text file.

In the measurement process, the Instron system and the Keithley system are not synchronized. Due to this, it is imperative that both segments of the test are started at the same time, and that the sampling rates in both system are the same. The combining and the post-processing of the data is done by a software written in MATLAB environment. In the MATLAB software, first the data from Instron data files and resistance data files are read. Next, the data is parsed so that all data relevant to one sample is arranged to

one structure. After this, the data can be processed and plotted in a desired way. For example, the resistance vs. strain figures can be plotted for each sample.

There are certain advantages and disadvantages in using this setup. The advantages are the precision in measuring the strain, and the possibility of also logging the load data in addition to the strain and resistance data. However, the disadvantage of this setup is its unreliability. The main problem lies in making the connection from the stretchable platform to the rigid resistance measurement wires. The clipper connectors cannot be directly attached to the stretchable pads, as the thin TPU substrate is quite fragile. A set of tests were done by using Nicomatic Crimpflex contacts. The other end of the contacts was pushed through the pad area, and this connection was further reinforced with Creative Materials 124-08C electrically conductive epoxy adhesive. 4 cm long wires were soldered to the other end of the Crimpflex contacts, and then the resistance measurement wires attached to these wires with the clipper connectors. With this approach, approximately half of the measured samples were still working when they were attached to the test setup. With this connectivity method, the problem is in the small amount of available space below the static clamp. Due to the lack of space, the pad area may get some of the pressure when the clamps are closed. This results in cracking of the cured epoxy adhesive, which usually results in lost conductivity. However, also a certain type of press connector was experimented. This connector is presented in Figure 16.

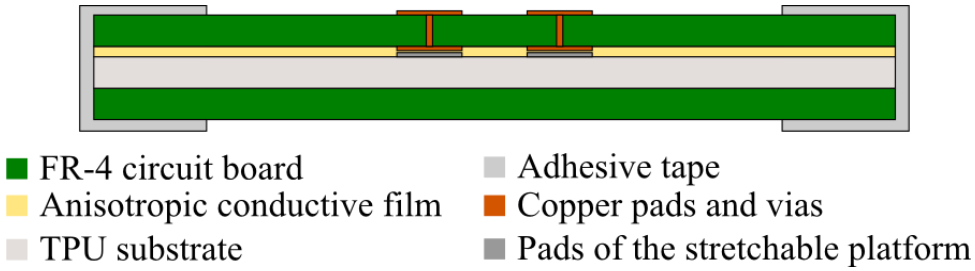

Figure 16. *Press connector used in the Instron 4411 –based test setup.*

In this connector, the stretchable platform is pressed in-between two pieces of rigid FR4 PCBs. On the other piece of rigid PCB, there are same-sized pads as those on the stretchable platform, and they are aligned so that connectivity is ensured between the matching pads. To ensure the electrical conductivity between the rigid and stretchable platforms, a layer of anisotropic conductive film (ACF) is attached between the two platforms. In addition, a couple of layers of adhesive tape were rolled around the ends of the connector to ensure its durability. To attach the measurement wires to this connector, small wires are soldered to the outer layer of the rigid PCB. With this method, approximately 70% of the measured samples provide reliable measurement results. The problems in this connector are mainly caused in the interface between the stretchable and rigid materials, which could be improved with an ACF that provides stronger adhesion.

4.3.2 Custom-Made Test Setup

Another take on the strain testing of electrically conductive materials is made in this thesis. In this case, the strain is controlled by a custom-made setup. This setup was originally implemented in Toni Liimatta's thesis, but it is further modified in this thesis [28]. The sample attachment area of the test setup is presented in Figure 17.

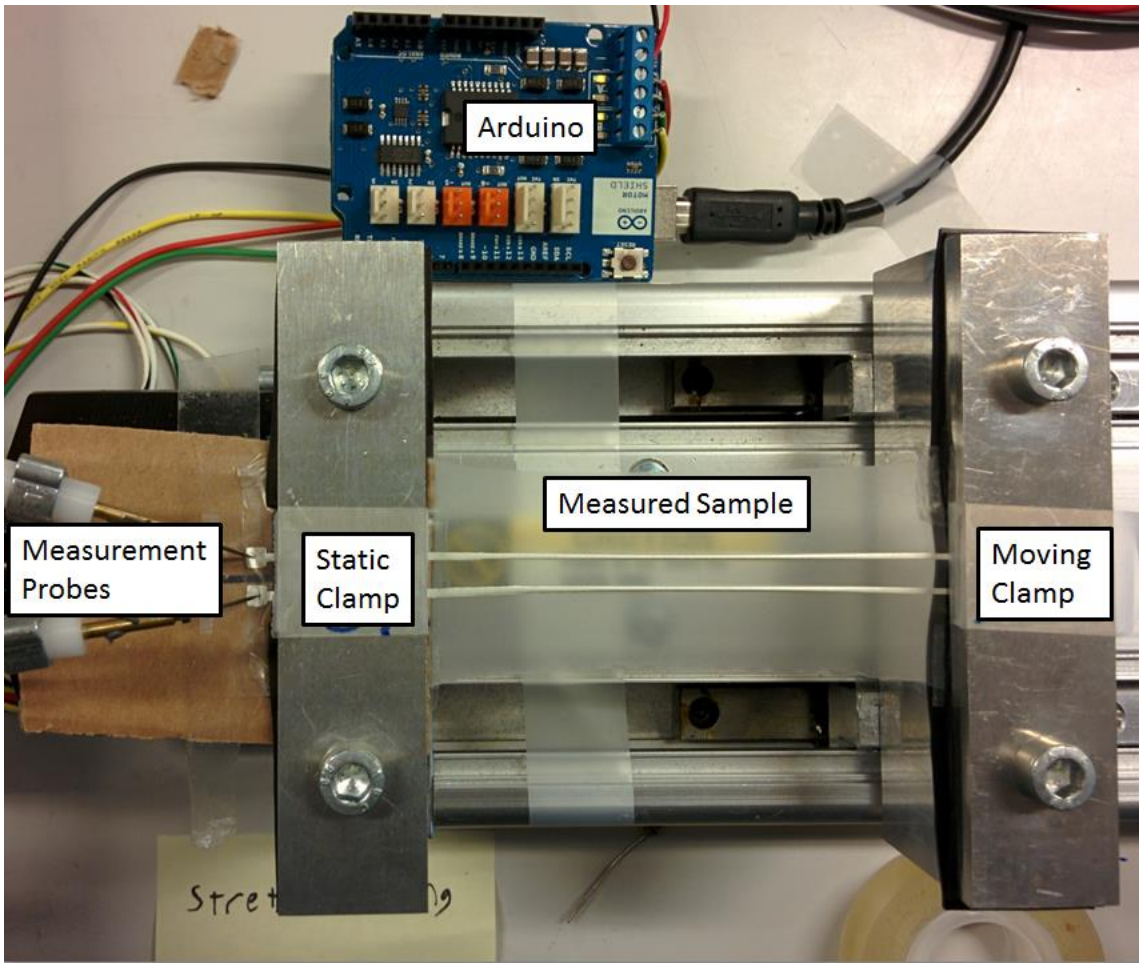

Figure 17. *The sample attachment section of the strain test equipment.*

In this setup, a linear actuator is used for causing the strain for the sample. The static clamp of this setup is at the other end of the linear actuator, and the initial location for the moving clamp is 61 mm towards the other end of the actuator. The strain-testing sample is placed so that the curve is under the moving clamp, and so that the pads go through the static clamp so that measurement probes can be placed on top of the pads. The sample is placed between two metal pieces, and the pieces are tightened together with hexagon socket screws. In the metal piece surfaces, there are 2 mm rubber pads in order to make sure that the sample will not slip away when the strain is increased. When the sample is properly the attached, the test may be started and then the moving clamp will start to move towards the other end of the linear actuator. An overall view of the test setup is presented in Figure 18.

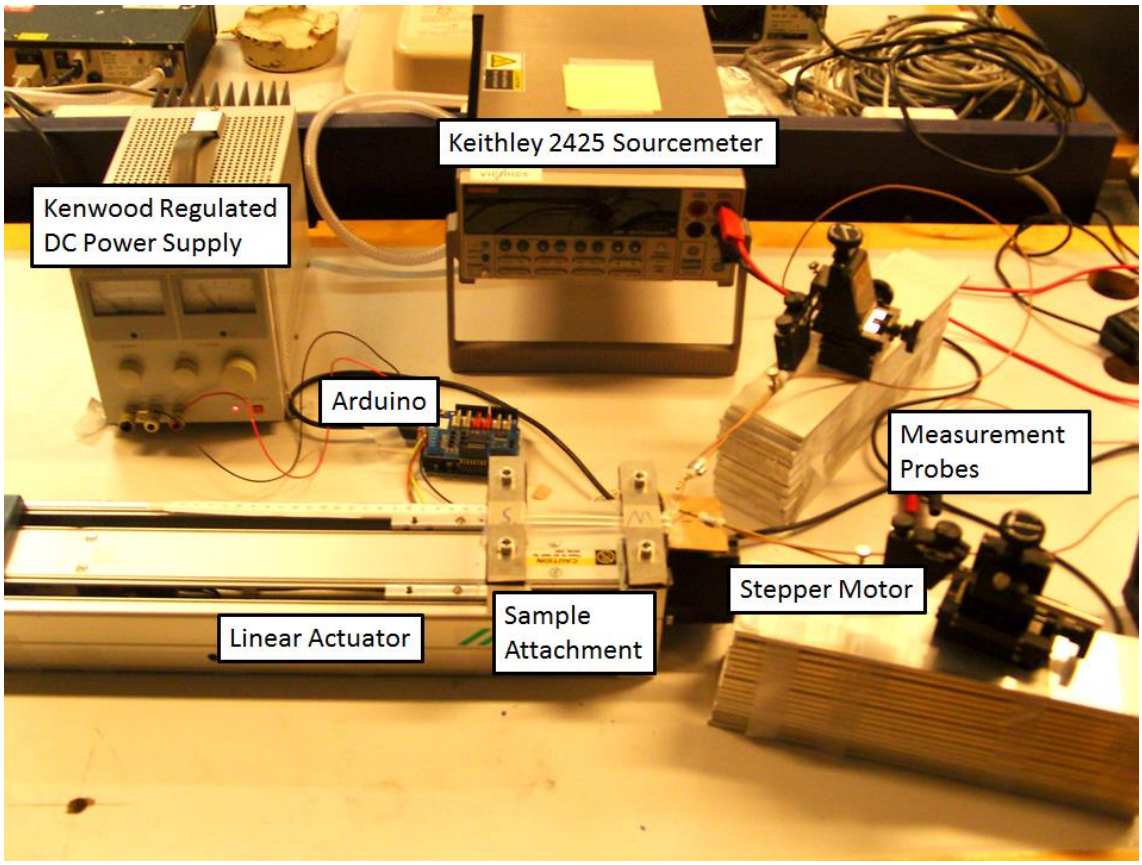

Figure 18. *The strain testing equipment.*

A Nanotec ST5709S1208 stepper motor powers the linear actuator. The stepper motor is controlled with Arduino Uno R3 open-source electronic prototyping platform with Arduino Motor Shield R3 attached. A supply voltage of 7 V is used for powering the motor, and it is provided by Kenwood Regulated DC Power Supply. The Arduino is connected to a laptop with an USB-cable in order to provide control over the strain with a serial connection. In addition, the Keithley 2425 Sourcemeter is also connected to the laptop over a General Purpose Interface Bus (GPIB) -USB cable.

The software required to run the test setup consists of two sections: LabVIEW software that runs on a laptop, and a software written in C language that runs on ATMega328P microcontroller on the Arduino. In the test setup, the Arduino acts as an interface between the laptop and the stepper motor. Its software provides a set of serial commands for the LabVIEW software, which result in driving the stepper motor accordingly.

The LabVIEW software controls the whole measurement setup, and its operation principle is presented in Figure 19.

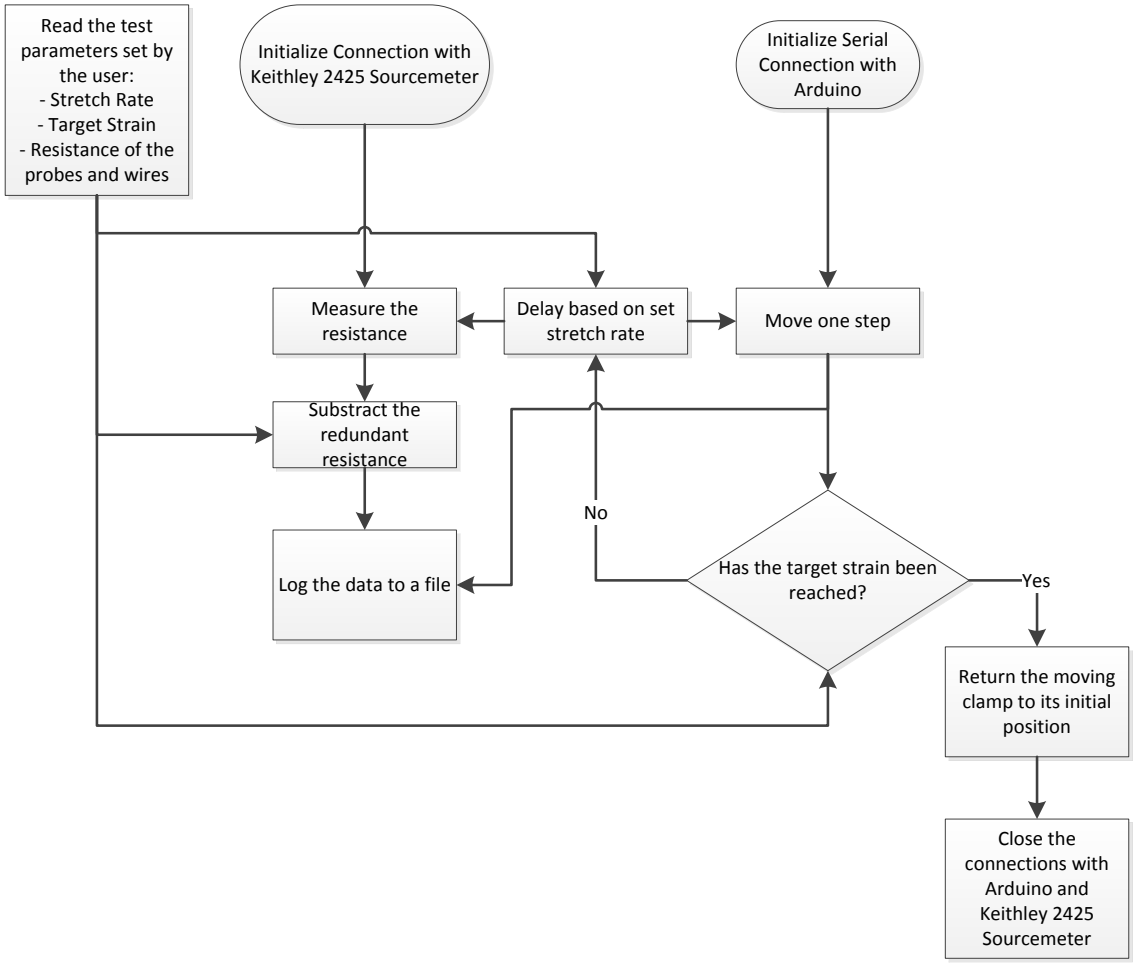

Figure 19. *The operating principle of the LabVIEW software.*

In the LabVIEW software, first the user can set the desired parameters for the test setup. These parameters are stretch rate in millimeters per minute, target strain as a percentage value, and the redundant resistances caused by the measurement wires. After the parameters are set and the sample is attached, the test may be started. At the start of the test, the program initializes connections with Arduino and Keithley. After this, the actual measurement is started. In each iteration of the measurement loop, the LabVIEW software sends a command to Arduino to drive the stepper motor one step. One step causes the stepper motor to rotate 0.90°. The screw lead of the linear actuator is 6 mm. Hence, when the stepper motor has rotated 360º, the moving clamp has traveled a distance of 6 millimeters. If one step of the stepper motor is 0.90º, it takes 400 steps for the moving clamp to travel the distance of 6 millimeters. So one step of the stepper motor results in 15 µm traveled distance of the moving clamp. This value together with the initial grip distance of 61 mm is used in the LabVIEW software to calculate the strain and log it to the data file after each step. In addition, for every step a command is sent to Keithley to measure the resistance, and this is logged to the data file as well for the matching strain. This is repeated until the target strain is reached, after which the data file is saved and the moving clamp is returned to its original position.

One advantage of this setup is the reliability of the sample attachment. Due to the horizontal placement of the linear actuator, the connection between the resistance measurement equipment and the measured is easily done by attaching needle probes on top of the pads. With this manner, none of the samples break in attaching them to the test equipment. Another advantage of this setup is that the desired resistance vs. strain data is available one a single file, which results in simpler post-processing. However, the main disadvantage of this setup is that the strain values are susceptible to error, as they are only calculated based on the issued move-commands and not measured. This causes a problem when the forces required for increasing the strain rise above a certain level, as this causes the stepper motor to skip steps which results in error in the strain values. The higher the strain is, the higher forces are and the more the stepper motor skips the steps. However, this error is systematic if the stretched material and pattern are the same, and can be reduced in post-processing. The amounts of error vs. strain when using the patterns and material combination of this thesis are presented in Figure 20.

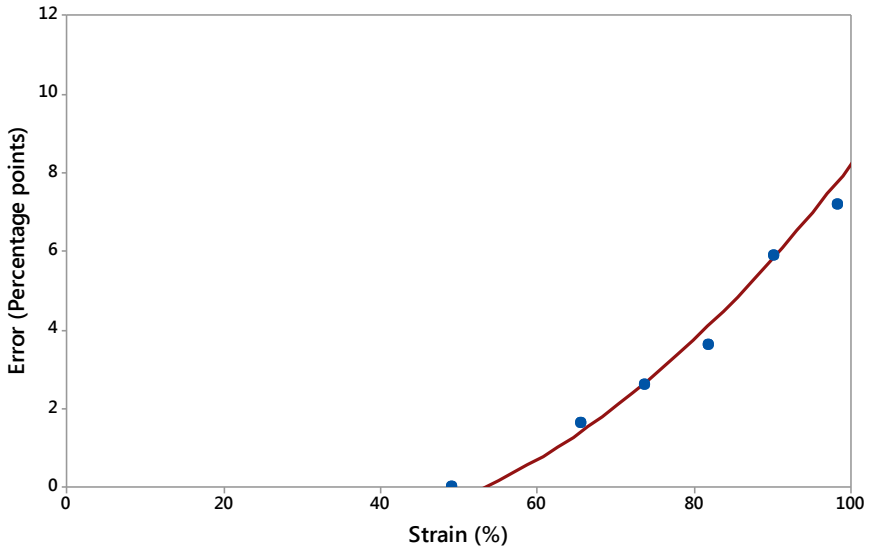

Figure 20. *Error vs. the strain present in the measurement setup when using the strain test samples of this thesis.*

The error presented in Figure 20 is an average of the measured samples, and the deviation is 2 percentage points as highest in the presented range. Therefore, after reducing the systematic error in the post-processing phase, a random error of 2 percentage points is still left.

4.4 Electromechanical Performance Measurement

In this thesis, the electromechanical performance of the stretchable interconnects is evaluated by doing single strain tests. For this test, three lots of 10 strain test samples are manufactured by screen-printing. Each sample is cut to a size of 38 x 140 mm^2, and

their initial resistances are measured before the strain tests. In addition, the traces are reviewed with an optical microscope to discover possible initial faults before the strain tests.

The custom-made test setup is chosen for the strain testing, due to the unreliability of the Instron-based setup. The samples are stretched until the conductivity is lost, and the stretch rate used in the tests is 2.5 mm/min. The resistance of each sample is measured throughout the strains from 0% to the point where the conductivity is lost. After the conductivity is lost, the samples are stretched approximately 5 percentage points more to ensure that the conductivity is not lost only temporarily. The purpose of this test is to discover the strains that are required to break the samples, and to evaluate the strain proportionality of the resistance. In addition, the data is used to further characterize the reproducibility of the screen-printing process.

With the custom-made test setup, another set of samples are also measured. In this test, 10 samples are stretched up to 100% strain. The setup is modified for this test so, that Olympus SZX9-stereomicroscope is placed over the linear actuator by using Olympus SZ-STU2 universal stand. In this test, the stretching is paused every 5 percentage points of strain and the trace is reviewed with the microscope. The purpose of this test is to discover the amount of strain required for the conductive traces to start cracking. This information is valuable for estimating the reliability of the stretchable interconnects in the use where the average strain are known, such as in smart garments. Additionally, this information can be used in designing the future reliability tests, such as cycle testing.

4.5 Mechanical Performance Measurements

The mechanical performance of the stretchable interconnects is also evaluated in this thesis. The purpose of the mechanical tests is to discover the loads required to stretch the interconnects, to discover the amount of permanent deformation caused by the strain, and to find the softening and hysteresis effects of the TPU when there are printed traces on its surface. Instron 4411 Universal Testing System is used for this testing. For this test, 10 samples of strain testing patterns are used. These samples are also cut to the size of 38 x 140 mm^2. The used grip distance in this test is 55 mm, and the stretch rate is 2.5 mm/min.

In the tests, each sample is stretched 5 times to 100% strain. After the first sample is stretched to 100% strain, the transverse length of the sample is measured to discover the Poisson's ratio for these patterns. After the transverse length is measured, the strain is released and the plastic deformation is measured once immediately, and once after 1 minute. This is done to verify the hysteresis of TPU. After this, the sample is stretched up to 100% four more times, to discover the softening property of TPU. After the last

stretch cycle is done, the plastic deformation is measured once more to discover if the additional cycles have effect on the plastic deformation.

5. RESULTS AND DISCUSSION

In this chapter, the results obtained by the experiments, test setups, and measurements discussed in chapter 4 are presented and discussed. First the limits of the printing process and used material combination are discussed. Next, the initial electrical properties of the stretchable interconnects and the performance under strain are evaluated. In these tests, also the reproducibility of the printing process is evaluated. Last, the mechanical properties of the interconnects are discussed.

5.1 Printability

In the printability test, several different test patterns were printed. First set of test patterns include line widths and gaps from 100 µm to 1000 µm with 50-µm step size in angles of 0°, 22.5°, 45°, 90°, and 112.5°. After printing, each of the samples was reviewed with an optical microscope. On the review, from each sample the narrowest successful line width was sought. In other words, all the narrower line widths than this line width are not successful in the printed pattern, and all the wider lines are successful. An example microscope image of successful and unsuccessful lines is presented in Figure 21.

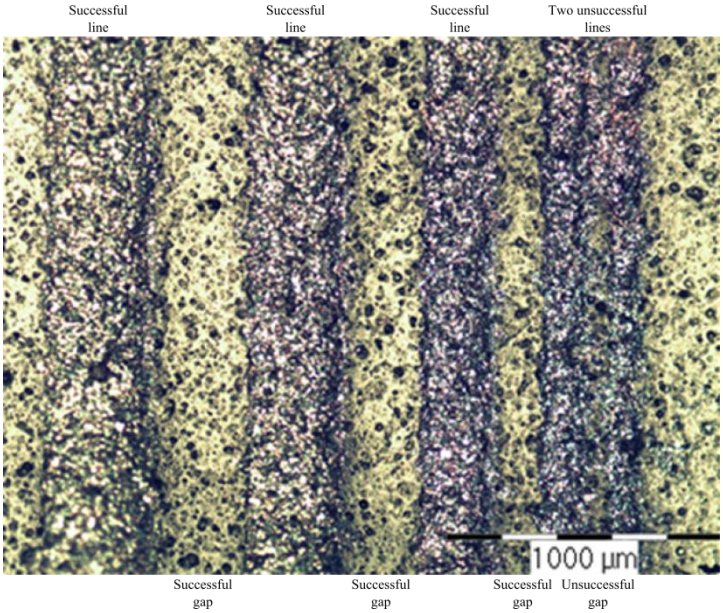

Figure 21. *Example microscope image of successful and unsuccessful lines. The two lines on the right are unsuccessful, as they have overflowed over the gap between them. The three on the left are successful.*

A line is considered successful if the line looks uniform and there are no overflows between the adjacent gaps. Hence, the narrowest successful gap for each pattern is 50 µm narrower than the narrowest successful line. Cumulative Distributon Functions (CDF) for each angle's throughput yield is presented in Figure 22.

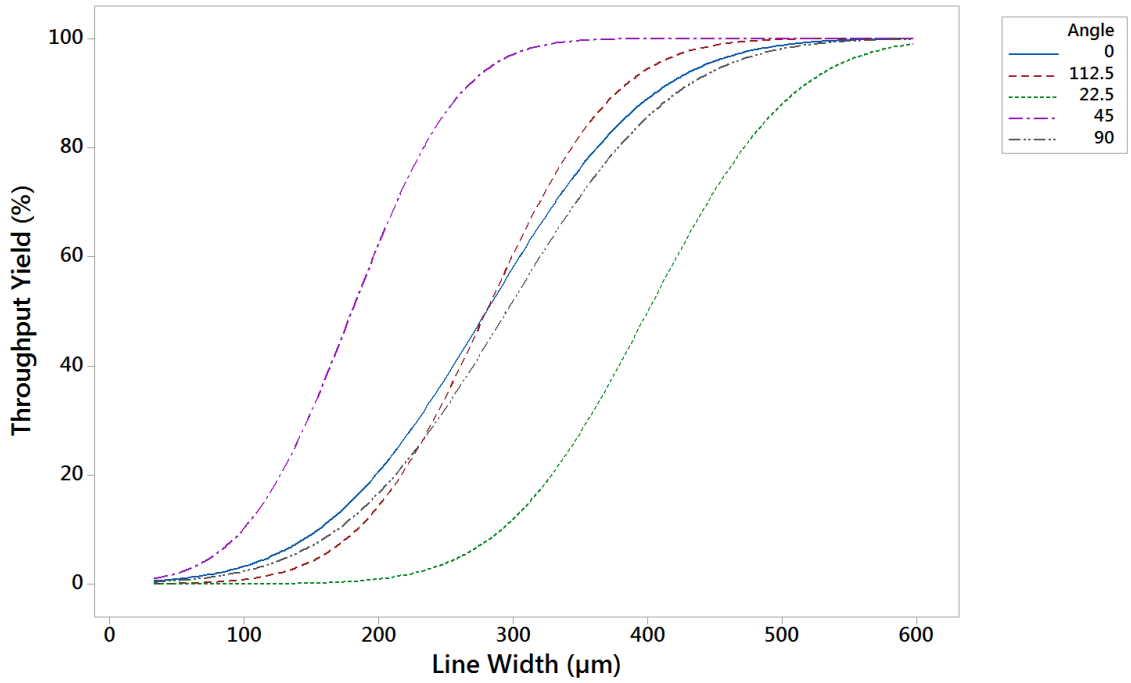

Figure 22. *Throughput yield's proportionality of the line width with different pattern angles. 10 samples have been measured of each angle.*

Based on these resuls, the 22.5° angle is the least suitable for printing narrow lines, and 45° is the most suitable one. However, a complex circuit pattern can have any combination of these angles. In that case, the yield will depend on the distribution of different angles used. Based on this study, for an arbitrary pattern where each of these angles are presented equally, the minimum line width that can be used to reach 95% throughput yield is 440 µm. Additionally, for 95% throughtput yield minimum gap width is 390 µm.

In the another set of test patterns, meander-shaped lines with 200 µm, 300 µm, and 400 µm widths and equal width gaps between them are printed in 0° and 90° angles. Also, capacitor-shapes are printed with same parameters. These patterns are first evaluated by measuring the conductivity between the pads, and if the resistances indicate problems they are further reviewed with microscope. For the meander-shaped patterns, if there is no conductivity, it can be determined that the lines are cut from somewhere. In addition, if the resistances were lower than the average resistance minus the standard deviation, it may indicate overflows that cause shortcircuits between adjacent lines. For the capacitor-shaped patterns, if there is conductivity between the measurement pads, it can be determined that there are flows that cause shortcircuits between the adjacent lines.

In reviewing the meander-shaped patterns, it was found out that each of the patterns were conductive. However, some of the patterns had shortcuts between the adjacent lines. Shortcuts were also found in capacitor-shaped patterns. A bar chart of the yields of these patterns is presented on Figure 23.

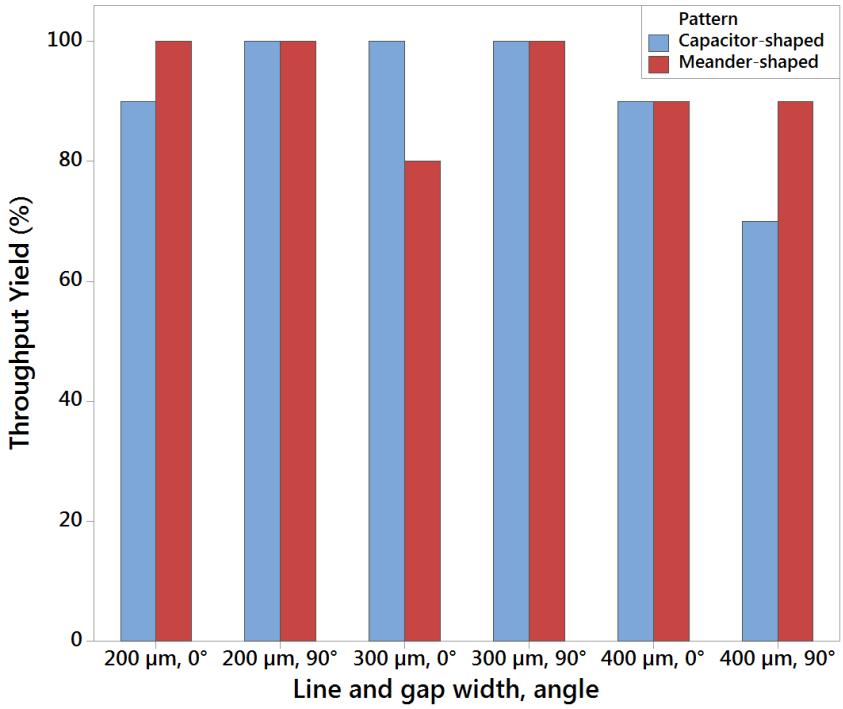

Figure 23. *The throughput yields for meander-shaped and capacitor-shaped patterns with different line widths, gap widths, and angles.10 samples have been measured of each shape and line and gap width.*

Based on the meander-shaped patterns, the 200 µm line has a higher throughput yield than 300 µm and 400 µm ones. The most likely reason for this is the printing parameter optimization; the parameters were optimized for the 200 µm patterns and the same parameters were used for the whole setup. The optimal squeegee pressure for printing 200 µm lines causes overflows for wider linewidths. In addition, these results are in contradiction to the review of printing the patterns presented in the first set, where this order of yield was reached only with line widths higher than 400 µm. The most likely cause for this is also the squeegee pressure. The meander-shaped lines are located near the edges of the screen, while the patterns of the first set are located on the center. Due to the softness of the rubber squeegee and the strength of the polyester mesh of the screen, the pressure is higher on the center of the screen than on the edges. Additionally, on these patterns there is a wider opening area on the screen through which the ink is deposited. The higher amount of ink on the area together with the higher squeegee pressure are the most likely reasons for the narrower line widths to be flooding.

The feasible gap widths were evaluated by using the capacitor-shaped patterns. In reviewing these patterns, a sample was determined unsuccessful if there is conductivity

between the pads. Based on these patterns, gap widths of 200 µm are feasible with high yield. This is also in contradiction with the review of patterns of the first set, where this order of yield was reached only with gap widths of 390 µm. And like with the meander-shaped patterns, the reason for this is also in the printing parameter optimization. Example microscope images of the patterns printed in this study are presented in Figure 24.

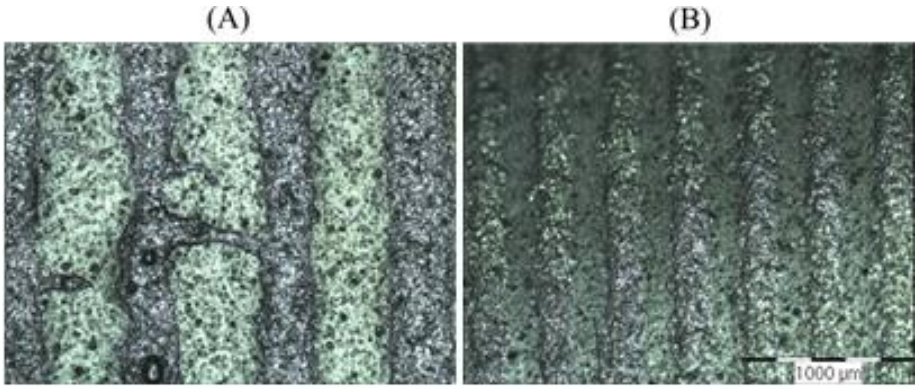

Figure 24. *Example microscope images of the printed patterns. (A) Overflow on a 400 µm capacitor-shaped pattern. (B) Successfully printed 200 µm meander-shaped lines.*

In conclusion, 200 µm line widths and 200 µm gaps are feasible with the used screen-printing process and material combination, when the printing parameters are optimized. However, in the case of a complex pattern where a wide variety of line widths and gap widths in variety of angles is present, finding the optimal printing parameters may be problematic. Based on this study, to reach 95% throughput yield in the manufacturing process, the minimum line width that can be used is 440 µm and the minimum gap width that can be used is 390 µm.

5.2 Performance and Reproducibility of Stretchable Interconnects

For evaluating the electrical and electromechanical performance of the stretchable interconnects, 30 samples of strain test pattern are manufactured. In addition to reviewing the electrical and electromechanical properties, also the reproducibility of the screen-printing process and testing is evaluated in this chapter. The samples were manufactured in three lots of 10 samples, and the properties for each lot are presented in Table 5.

Table 5. *The properties of the printed lots.*

Population	Number of samples	Ink	Substrate	Printing parameters	Printing operator	Printing Day
Lot A	10	ECM CI-1036	Epurex Platilon U4201	High pressure, two printing cycles	Operator 1	Day I
Lot B	10	ECM CI-1036	Epurex Platilon U4201	High pressure, two printing cycles	Operator 2	Day II
Lot C	10	ECM CI-1036	Epurex Platilon U4201	High pressure, two printing cycles	Operator 2	Day III

As can be noted from Table 5, the differences between the printed lots are that the manufacturing process of each lot is executed on separate days, and that Lot A has been manufactured by different operator than Lot B and Lot C.

5.2.1 Initial Electrical Performance of the Stretchable Interconnects

To review the reproducibility of the manufacturing process, the deviations between the samples and between the lots are reviewed with statistical analysis. A histogram of the sheet resistances with normal distribution fit is presented in Figure 25.

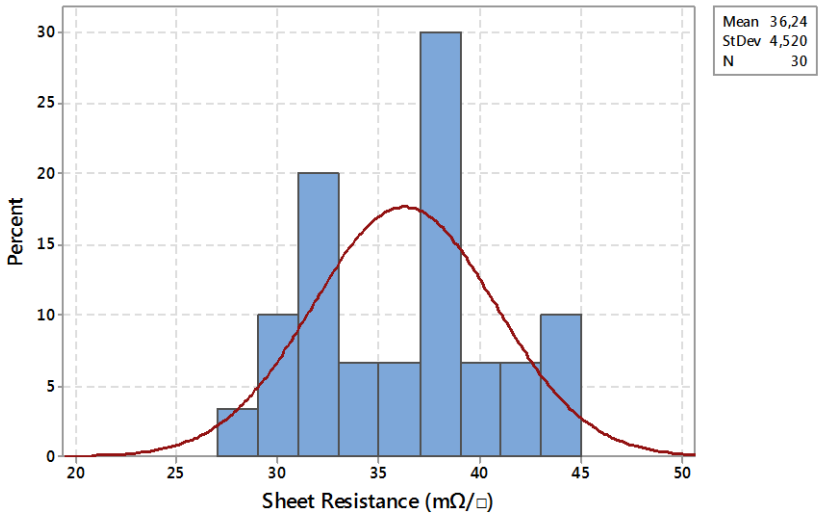

Figure 25. *A histogram presenting the distribution of the sheet resistances.*

The sheet resistances of the whole population vary between the values of 27 $m\Omega/\square$ and 45 $m\Omega/\square$. According to the datasheet of the ink manufacturer, the ink should provide lower than 10 $m\Omega/\square$ sheet resistances after curing. The maximum error of the sheet resistance measurement is 12.5%, and hence does not cover this difference. The difference is not further studied in this thesis, as the resulting sheet resistance is sufficient. However, this should be studied in the future by examining the thickness of the printed traces with for example interferometry or atomic force microscopy (AFM) and comparing these with the values of the ink's datasheet. Nevertheless, the mean value of 36.3 $m\Omega/\square$ surpasses the most of the initial electrical performances of the most stretchable interconnect material and strategy –combinations reviewed by Yao and Zhu [21]. The normality of the distribution is further reviewed in Figure 26.

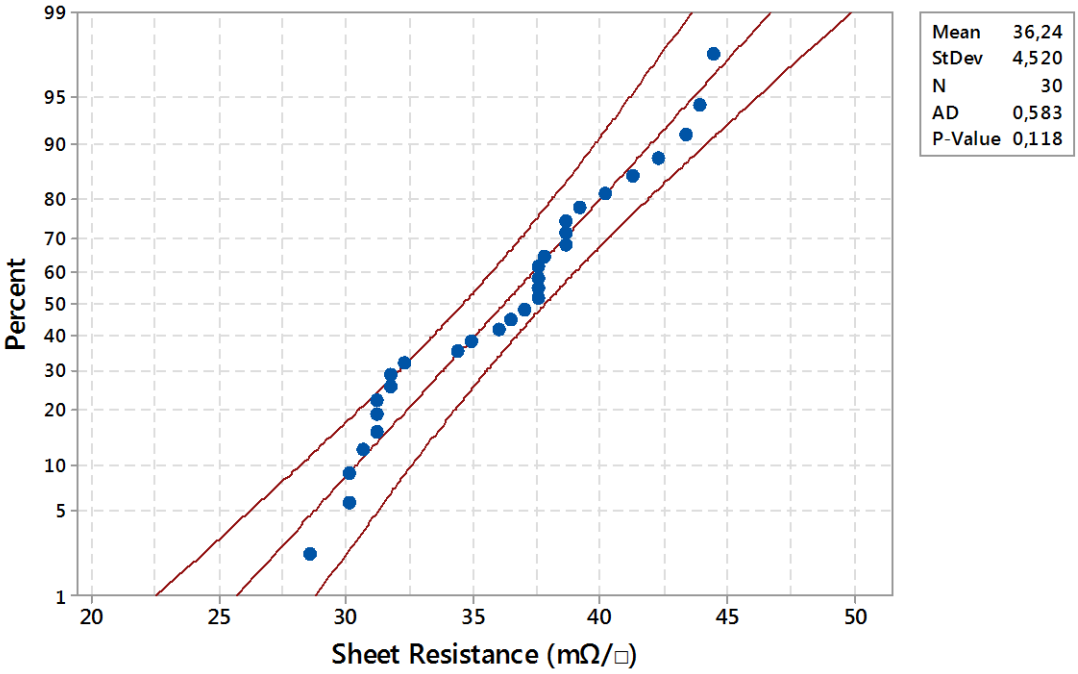

Figure 26. *Probability plot of sheet resistance with 95% confidence interval (CI) lines.*

In Figure 26, the population is tested if it is normally distributed. The null hypothesis is that the data is normally distributed. Typically, a threshold of 0.05 is used for the P-value. If the P-value is lower than 0.05, the null hypothesis should be rejected. As the P-value is over 0.05 in this case, it can be concluded that the population is normally distributed. The Anderson-Darlington (AD) statistic can be used to evaluate the fit to the distribution, and to compare different distributions. The lower the AD statistic is, the better it fits the selected distribution. [29] However, to further understand the deviation in the process, the variation between the different lots should be reviewed. The histogram with separation between the different lots is presented in Figure 27.

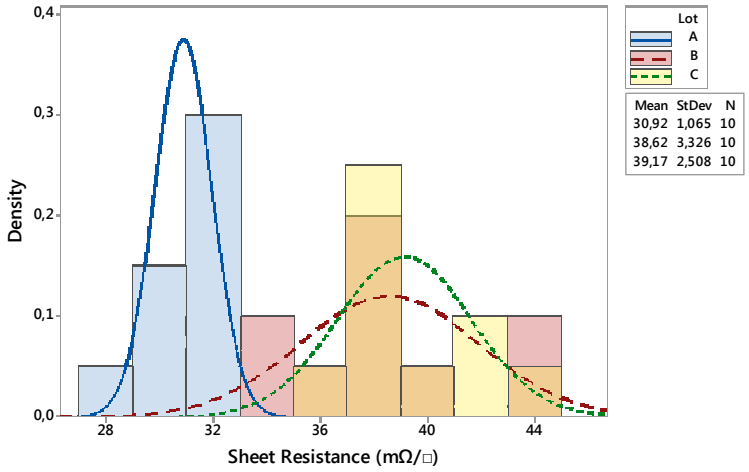

Figure 27. *A histogram of sheet resistances with separation between the different lots.*

From Figure 27, it can be noted that lot B and C are approximately the same, but lot A differs from these two lots. The distinguishing factor between these two clusters is that lot A and lots B and C are made by different operators, as can be noted from Table 5. In Figure 28, the probability plots for sheet resistances of each lots are presented in order to determine whether each subset is normally distributed.

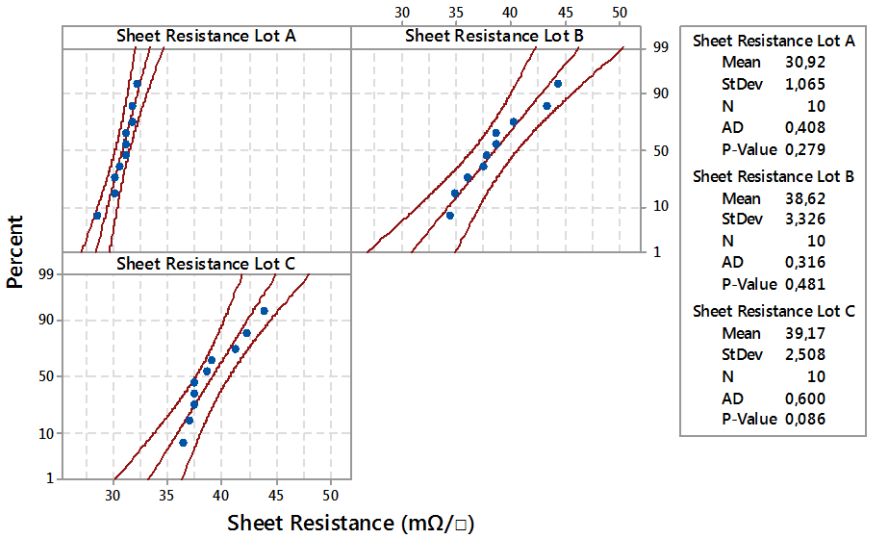

Figure 28. *Probability plots of sheet resistances for different lots.*

Based on the P-values of Figure 28, the sheet resistance data of each lot is normally distributed. However, it should be noted that the P-value of lot C is low and the AD static is high in comparison to these values of other lots or the values for the whole population. This may be an indicator of some exception in the manufacturing process of certain samples in lot C, but this exception was not discovered from the data available.

The two-sample t-test is used to further compare the means of the different lots. The test is used to determine if the difference of the means between the lots is significant. In other words, the test can be used to determine if the compared lots can be seen as samples of the same population. In the test, two lots are compared at the time, and the results for these comparisons are presented in Table 6.

Table 6. *The results of the two-sample t-tests.*

Lot 1	Lot 2	P-value
A	B	0.000
A	C	0.000
B	C	0.679

In the two-sample t-test, the threshold used for P-value is 0.05. If the P-value is higher than the threshold, it can be concluded that there is no difference between the means. As can be noted from Table 6, lots B and C have no significant difference in the means, and stating the opposite has the probability of 67.9% of being wrong. As for lot A, it is clear that its mean significantly differs from the means of B and C. [30][31]

In conclusion, the initial electrical performance is satisfactory for the target application. However, in order to improve the sheet resistance of these samples, the next step is to measure the thickness of the samples. If the thickness is lower than the one specified in the datasheet of the ink, the thickness should be increased. In order to optimize the printing process and lower the deviation between the lots, the differences between the operators should be studied, or a printer with better possibilities to measure the printing parameters should be used.

5.2.2 Microscope Review of the Stretchable Interconnects

After measuring the sheet resistances and before the strain testing, the samples were reviewed with an optical microscope. In the review, the purpose was to determine if any faults exist in the traces that could increase the initial resistance or worsen the strain performance of the conductor. However, no faults were found during the review. In addition, the line width was approximately measured during the review. The edges of the trace are not straight, and this complicates the measurement. An example microscope image is presented in Figure 29.

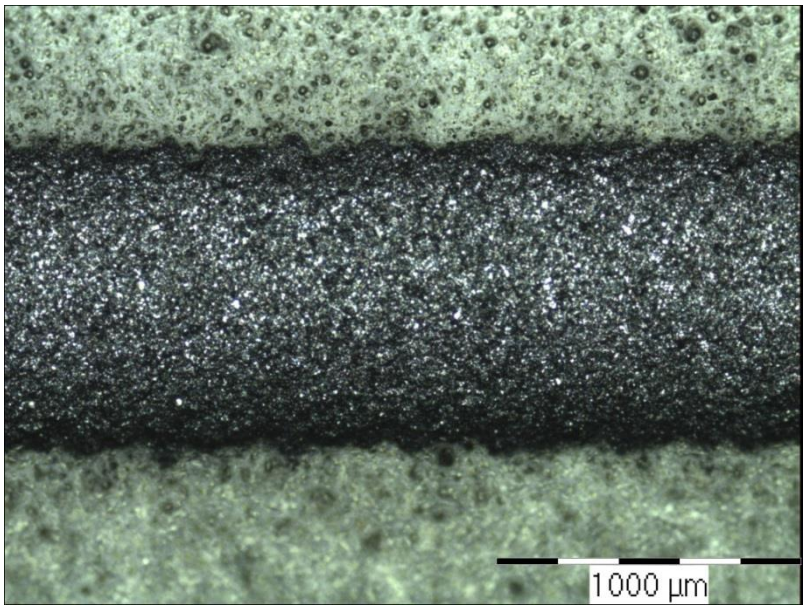

Figure 29. *A microscope image of the screen-printed strain test pattern.*

As the line width is measured from this pattern manually using an optical microscope, only the narrowest and the widest section is measured from each sample. A CDF of these values is presented in Figure 30.

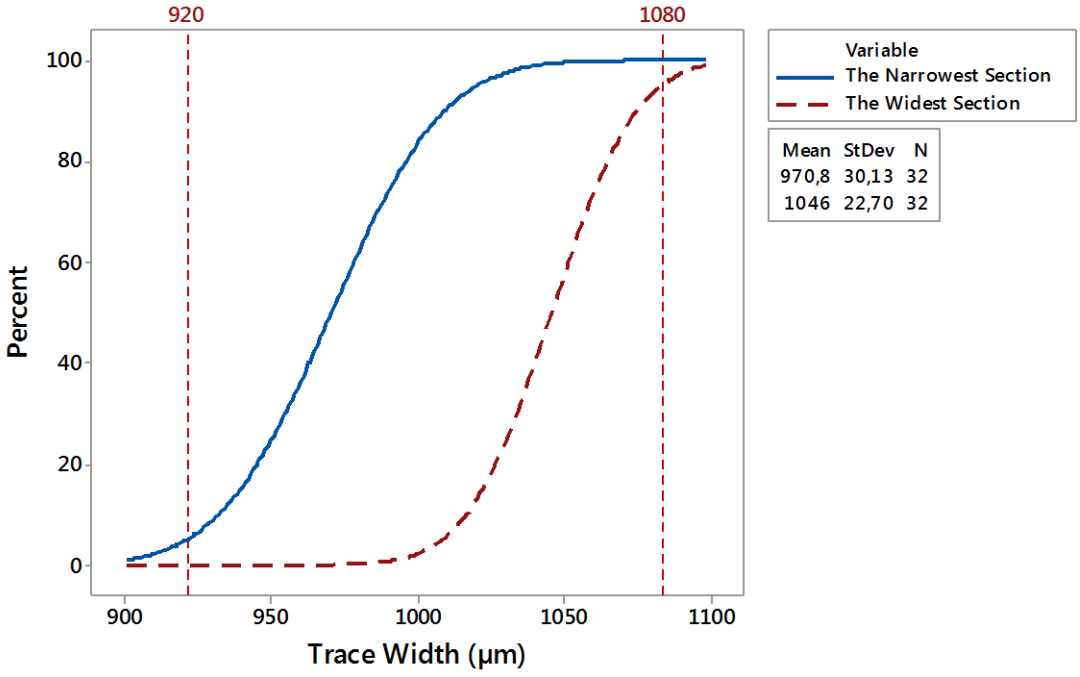

Figure 30. *A CDF of the measured narrowest and widest sections of the traces of the whole population.*

Based on Figure 30, there is a 95% probability that the line will not be narrower than 920 µm at any point, and a 95% probability that the line will not be wider than 1080 µm

at any point. Based on this information, 100 µm gaps are sufficient when printing 1 mm lines with screen-printing. In order to find connecting factors between measured resistances and the measured line widths in the future, more accurate measuring method should be used to find average values for the trace widths of each sample. For example, interferometry or AFM would provide more accurate results about the line width and the line thickness.

5.2.3 Electromechanical Performance of the Stretchable Interconnects

Each of the 30 samples was stretched up to the strain where they lost conductivity, and at least 5% over that point to ensure that the conductivity is not regained. The resistances were measured continuously during the stretching. An example of the proportionality between the resistance and the strain is presented in Figure 31.

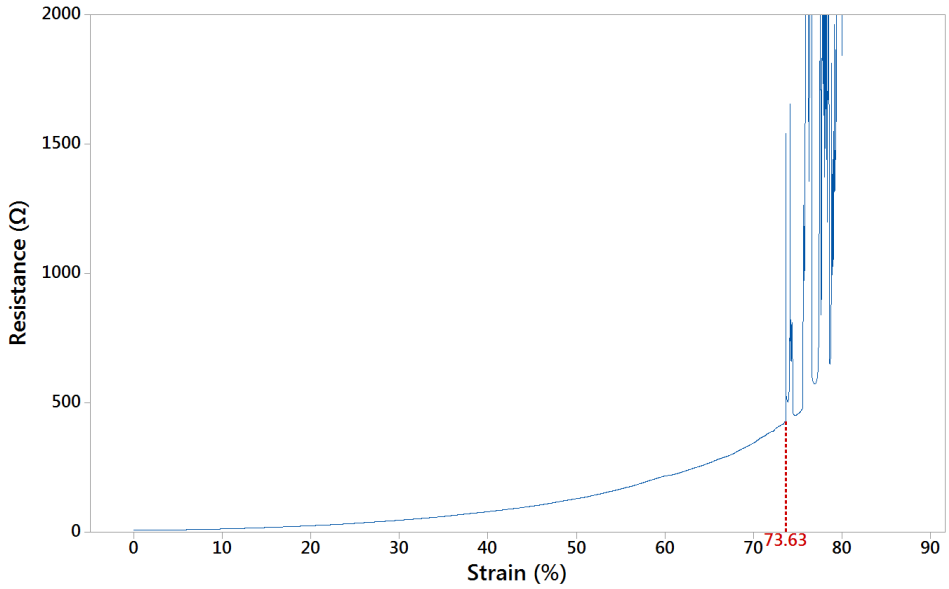

Figure 31. *Resistance vs. strain measurement for one sample from lot C. The red line represents the break point of the sample.*

In most of the cases, the resistance grows rapidly even up to several kilo-ohms before the conductivity is lost. In this thesis, the break point is defined as the lowest strain where condition

$$\frac{dR}{d\epsilon} \geq 5 \tag{8}$$

is satisfied. A derivative plot of Figure 31 is presented in Figure 32 in order to illustrate this further.

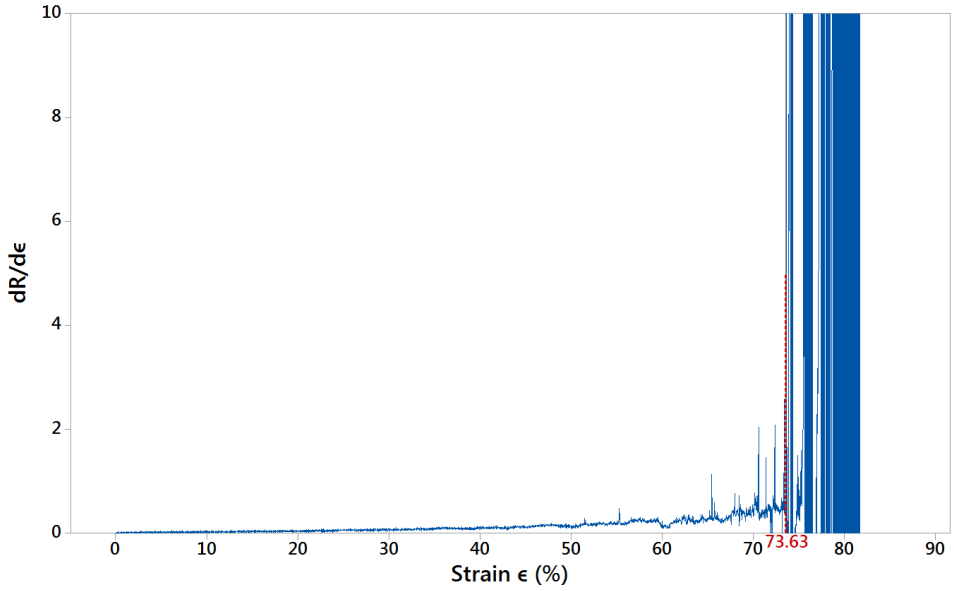

Figure 32. *The derivative of the resistance vs. strain from Figure 31. The red line represents the break point of the sample.*

As can be seen from Figure 32, the derivative starts to rise already before the actual break point, but the threshold is not exceeded before 73.63% strain. From Figure 31 it can be seen that at this strain the resistance starts to grow at a significant rate. However, there are also cases where the conductivity is lost without the rapid rise, and in these cases the break point is defined by the strain where the conductivity was lost. The threshold value of 5 has been found by a trial and error –process. In the process, first the break points of the population were searched by a MATLAB algorithm, which scanned through the data and provided break points based on the set threshold value. Then the accuracy of these found break points was reviewed by comparing these to the strain vs. resistance figures. This was repeated with several different threshold values, and the value 5 was chosen as it provided the most accurate results of the break point. With the same algorithm, the break points were searched for the samples of lots A, B and C, and a CDF plot of the break points is presented in Figure 33.

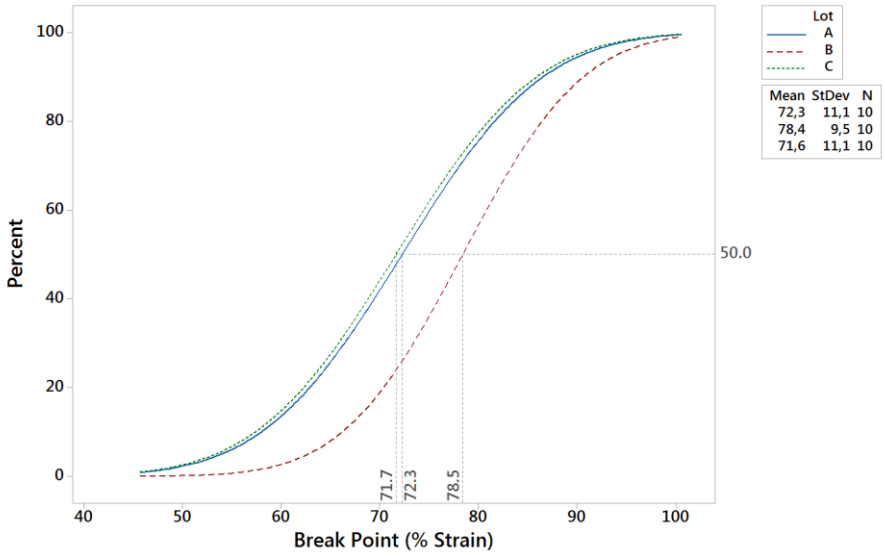

Figure 33. *A CDF plot of the break points for separate lots with 50% reference lines.*

Based on this data, 50% of the samples break at approximately 74.1 % strain. Lots A and C appear to have a similar stretch performance based on Figure 33, and lot B seems to be a bit different. However, a set of two-sample t-tests was done to compare the break points of the lots with each other, and for each test the p-value was higher than 0.05. Hence, in terms of stretch performance the lots are all the same, despite the difference between the lots in the initial electrical properties. This is explained by the definition of the break point, as it is calculated by the differentiating the resistance values.

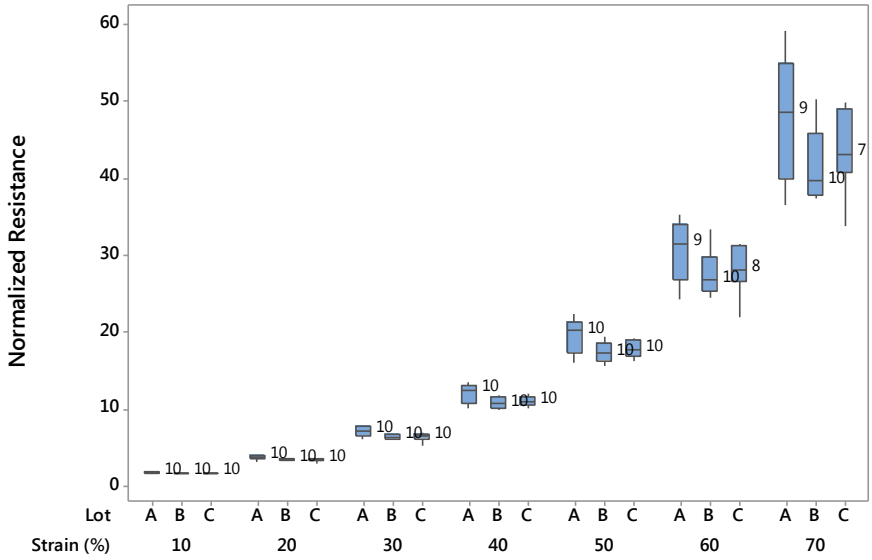

Figure 34. *Boxplot of normalized resistance vs. strain performance for lots A, B and C.*

In Figure 34, the resistance is normalized with each sample's resistance at 0% strain.

The whiskers of the boxplot represent the variance of the data, and the box represents the 50% of the sample set. The line crossing the box represents the median, and the number next to each box represents the number of measured unbroken samples. Based on this data, it can be seen that the resistance increases linearly up to 30-40% strain, and then the growth rate of the resistance starts to further increase. Also, it can be noted that the variance between the samples starts to gradually increase when the strain is increased.

In addition, the failure of the samples during the stretching was reviewed. An additional lot of 10 samples was manufactured with the same parameters as lots B and C. The samples were strained in the same test setup as the other lots, but a stereo microscope was added on top of the linear actuator. By using the Olympus SZ-STU2 universal stand, it was possible to move the microscope in order to cover the whole stretched area. In this test, the stretching was paused every 5% of strain, and the sample was reviewed with the microscope at each point. The purpose of this experiment was to find out the strain values where cracks start to emerge. In this thesis, the lowest value of strain where signs of cracking are found for the sample by optical review, is called the cracking point. A CDF for the cracking points and the points where conductivity is lost is presented in Figure 35.

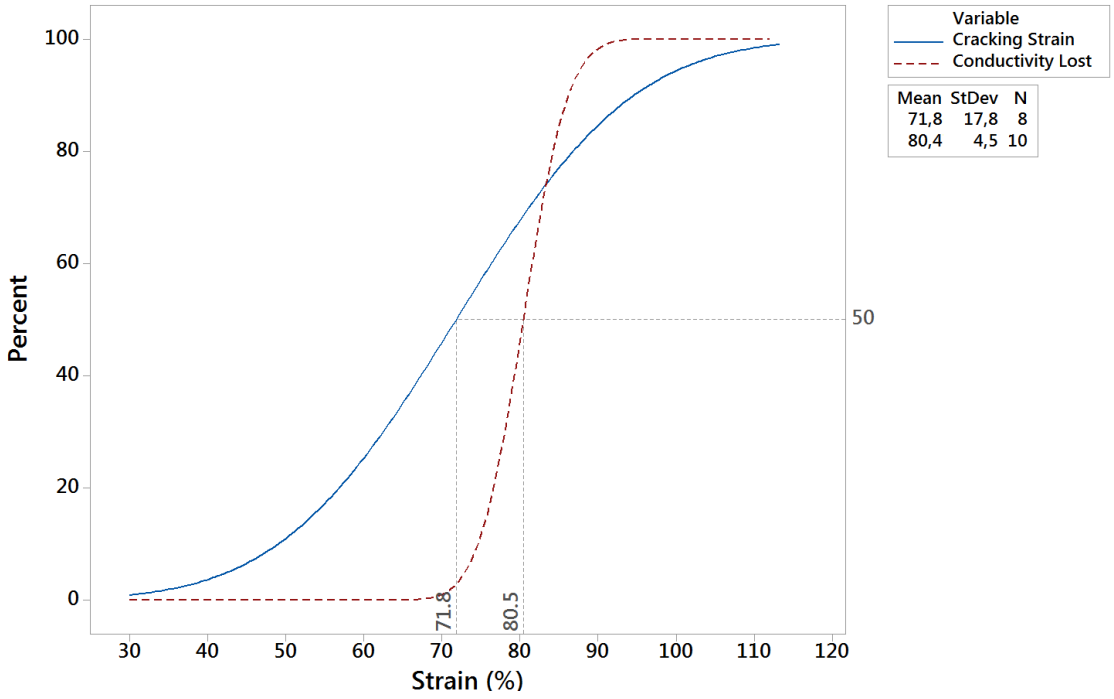

Figure 35. *A CDF plot of the cracking point and the point of conductivity lost.*

In Figure 35, the cracking point was discovered for 8 out of 10 samples. The remaining two samples lost conductivity before any cracks were discovered with the microscope. Based on the study, 50% of the samples start to show cracking at 71.8% strain and lose

conductivity at 80.4%. An example microscope image of a crack that emerged during the strain test is presented in Figure 36.

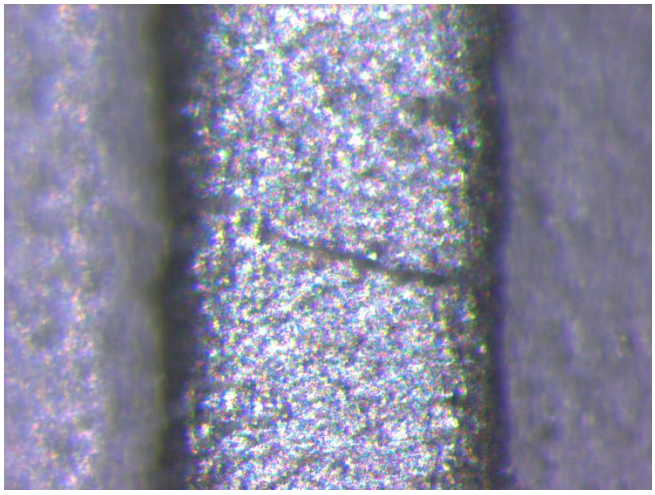

Figure 36. *An example microscope image of a crack which emerged during the strain tests. The sample is stretched to 70% strain in this image.*

In conclusion, the target strain of 30% is reached with ease on these stretch tests. The samples start to break at 45-50% strain at the earliest based on the tests, and only one sample showed any cracks at 30% strain on the cracking study. Also, the growth of the resistance is very linear up to 30%. However, to further understand the durability and the recovery of the interconnects in the strain range, cycle tests between strains 0% and 30% should be done in the future. The printing process used can be utilized to manufacture satisfactory stretchable interconnects for the target application. However, the initial electrical properties and the reproducibility of the printing process should be improved in the future.

5.2.4 Mechanical Performance of Stretchable Interconnects

In the mechanical evaluation of the interconnects, the forces required for the stretching are measured, and how each stretching cycle affects these forces. 10 samples are used for conducting these tests. An example of this behavior is presented in Figure 37.

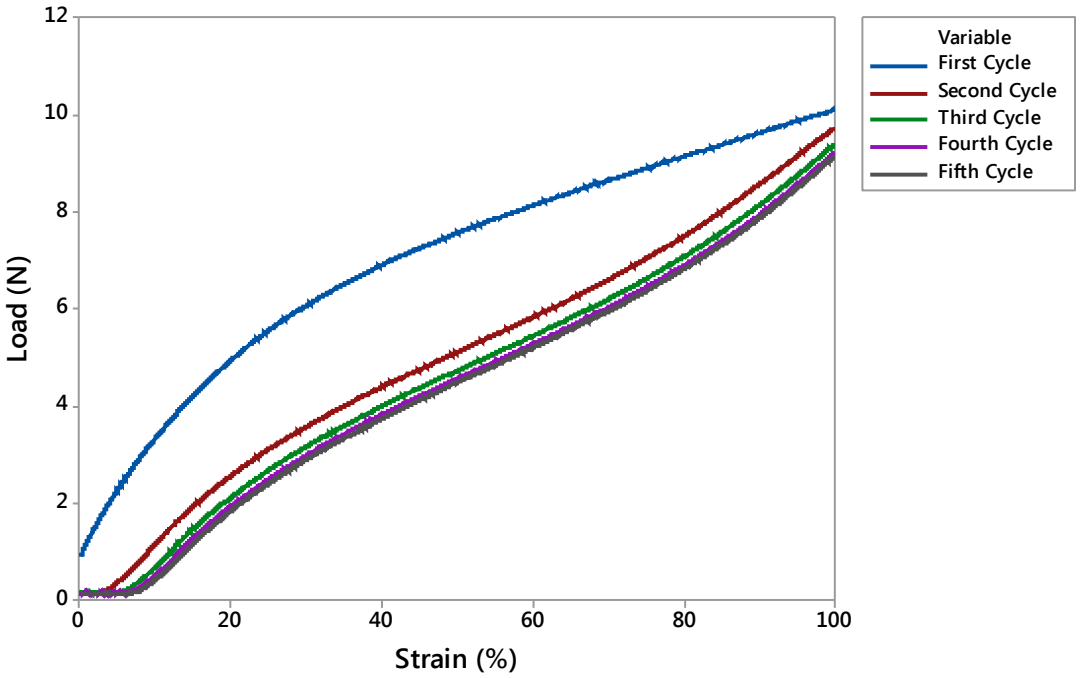

Figure 37. *An example of how five stretch cycles affect the load required for the strain for one sample.*

As can be noted from Figure 37, the forces exhibit the softening effect that is typical for the TPU substrate. After the first cycle, the forces required for the strains drop significantly, and as the number of cycles increase the change decreases and the sample starts to reach an equilibrium state. The change in the required force is especially significant in the strain area of 0-30%. Hence, in order to increase the unobtrusiveness and comfortability of the TPU interconnect in textile-integrated electronics, pre-stretching the substrate before printing might be worth to study. However, it is important to note that the strain-stress behavior is likely to change significantly when the stretchable interconnect is attached to the textile, and hence the strain-stress behavior of the textile, and the combination of the textile and the stretchable interconnect should be studied as well.

All the 10 samples present the similar of behavior as the one measured in Figure 37. For each of the samples, the Poisson's ratio was also measured to be v = 0.7. This information can be used to characterize how much the traces bend when the interconnect is stretched, and may be useful if this is simulated in the future. However, to make the simulations viable for variety of patterns, the deformation parameters should be further studied in the future. These could include the Poisson's ratio for only the used TPU, and Poisson's ratio for a sheet where the surface of the TPU is filled with the used ink.

In addition, as may be seen from Figure 37, the elastic region of the TPU ends already at approximately at 15-20%, and after this the permanent deformations start to occur. The residual strain was measured immediately after the first cycle, one minute after the

first cycle, immediately after the fifth cycle, and one minute after the fifth cycle. The reason for waiting one minute was to confirm the hysteresis effect of TPU. The results of this measurement are presented in Table 7.

Table 7. *Results of the residual strain measurements.*

Residual Strain	Immediately after the first cycle (%)	One minute after the first cycle (%)	Immediately after the fifth cycle (%)	One minute after the fifth cycle (%)
Average	11.3	8.6	15.2	12.4
Standard deviation	1.5	1.5	1.3	1.2

As can be noted from the results in Table 7, a significant residual strain is caused by the stretching. However, as it can be noted that the residual strain decreases over time, it is confirmed that the hysteresis effect of the TPU exists in these strain test samples.

In conclusion, the samples exhibit the typical performance for TPU substrate. There is a high possibility that the residual strain causes an increase in the resistance when there is no load applied to the interconnect, but also it is likely that the resistance decreases over time as the residual strain decreases. It should be further studied how does the behavior of TPU reflect on the electrical performance of the interconnects. In addition, the effect of pre-stretching these interconnects, and the stress-strain behavior of the textile-integrated stretchable electronics should be further studied.

5.3 Textile-integration Demonstration

In this thesis, a short demonstration was done to experiment the textile-integration of the stretchable interconnects. This experiment is presented in Figure 38.

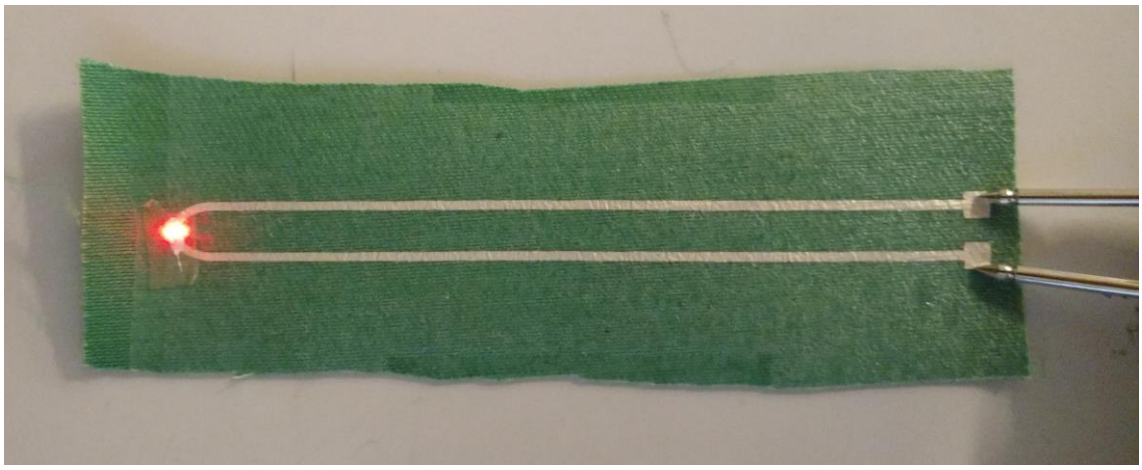

Figure 38. *A textile-integration demonstration.*

In this demonstration, a strain-test pattern printed with the ECM CI-1036 ink on the Epurex Platilon U4201 TPU is integrated to a piece of textile. The textile-integration is done by placing the TPU on the textile, and then by applying heat and pressure on the area. The temperature is approximately 170 ºC, which is in the softening range of the used TPU substrate. Then, pattern is cut from the curve, and an surface-mount device (SMD) LED is placed over the cut. The LED is then connected to the conductive traces by applying a small amount of the ECM CI-1036 ink between the pads of the LED and the traces, and then by curing the circuit in the oven. The circuit in Figure 38 is powered by a multimeter in diode test mode.

6. CONCLUSIONS AND PROPOSALS FOR FUTURE WORK

In this thesis, the objective was to manufacture stretchable interconnects by screen-printing, and to characterize these interconnects. This objective was reached.

In Chapter 2 of the thesis, the current situation of the wearable electronics market is reviewed, and some forecasts are covered. Several types of different wearable applications are presented, mostly in the sports and healthcare industries. One of these applications is the shirt capable of measuring bioimpedance, which is the deliverable of the project for which this thesis work is also done. Hence, in this thesis the requirements of this application, such as biocompatibility, comfortability, and textile-integration possibilities are considered in the material choices. It was discussed that the stretchable interconnects are required to endure at least 30% strains in the textile-integrated applications.

In the Chapter 3 of this thesis, first the advantages of using stretchable electronics in wearable electronics, such as unobtrusiveness, are discussed. The mechanics of elasticity required to characterize the stretching performance of the interconnects are also covered. Next, the principles of implementing stretchable electronics that are found in the literature are reviewed. These include commonly used materials for substrates, advanced materials for making the conductive traces, and special techniques and geometries that can be used to render conventional conductors stretchable. Last in this chapter, the theory of the screen-printing is covered.

The limits of the screen-printing process and the chosen materials are first reviewed in the Chapter 4. The limits are the thinnest line widths that can be printed with 95% throughput yield. These limits are searched for by using different test patterns that have different line widths in different angles. After the printing is done, these patterns are measured with an optical microscope. In addition, some of the patterns are reviewed with conductivity tests. Next in Chapter 4, two different stretch-testing setups are designed and experimented. In the first implemented test setup, Instron 4411 Universal Testing System is used for controlling the strain of the tested stretchable interconnects. While the strain is increased at a constant rate, the resistance of the interconnect is continuously measured with Keithley 2425 sourcemeter, and the data is logged with a LabVIEW-software. In the end, the strain and resistance data are combined with an MATLAB algorithm. The second test setup uses the same resistance logging system, but the strain is controlled with a stepper motor powered linear actuator. The stepper

motor is in this case also controlled with the LabVIEW software, and an Arduino electronic prototyping platform together with a motor shield is used to interface between the computer software and the stepper motor. Both of the setups have their advantages and disadvantages. The advantage of the Instron-based setup is that it provided data about the forces required to cause the strains, and that it has high precision control over the strain testing. The disadvantage is that the electrical connections attached to the stretched sample are unreliable, and due to this approximately half of the samples break before the test. For the another setup, the advantages are that the electrical connection is easy to make and hence reliable results can be measured from approximately all the samples manufactured. The disadvantage is that the strain measurement is prone to error, as the strain is calculated and not measured. By using fixing tables, the systematic error can be reduced, but the random error of two percentage points persists. In the measurements of this thesis, the initial electrical properties for all the samples used for stretch testing are measured. In the strain tests, both of the presented test setups are used. The mechanical properties of the interconnects are measured with the Instron 4411 –based setup, and the electrical performance during the stretching is measured with the other test setup.

The results of the experiments presented in Chapter 4 are presented and discussed in Chapter 5. First, the results of the printability tests are presented. Based on these results, 200 µm line and gap widths are feasible with the used printer and materials. However, it was determined that if the desired pattern includes variety of different line and gap widths in several different angles, the optimization may get complicated. Hence, to reach a 95% throughput yield with this process for such a pattern, a minimum line width of 440 µm and minimum gap width of 390 µm should be used. As for the differences in the angles between the process direction and the pattern, angle of 22.5° provided least successful, while 45.0° provided the best results.

Before doing the strain testing for the samples, the initial electrical properties for these 30 samples were first measured. The sheet resistances of the samples had a mean value of 36.3 $m\Omega/\square$, with a standard deviation of 4.5 $m\Omega/\square$. In the strain testing, approximately half of the samples break at a strain of 74.1%. Until the 30-40% strain, the resistance of the samples increase linearly, and from this point onward the growth rate of the resistance starts to gradually increase until the samples break. Based on these samples, it seems that initially the required strain of 30% is reached with ease. Additional 10 samples were manufactured, and they were also stretched up to the point where they break. These samples were reviewed after every 5% of strain with an optical microscope in order to discover when the samples start cracking. Half of the samples had started cracking at approximately 72% percent, and the earliest one started at 30%. Based on this study, these interconnects should provide sufficient durability in the textile-integrated applications where the strains are in the order of 20%. However, to be certain of this durability, cyclic tests should be performed for these interconnects in the future.

In addition to the electrical properties, the reproducibility of the manufacturing process was evaluated by statistical analysis performed on the sheet resistances. It was discovered that with the printer used in the manufacturing, the results are different depending on the operator who performed the process. This happens due to the lack of precision in controlling the printing parameters. To lower the deviation in the process, either the differences between the operators' actions should be studied, or a printer with better control over the parameters should be used.

Also, the mechanical properties of the interconnects were measured with the Instron 4411 Universal Testing System. Each sample was stretched up to 100% strain five times to confirm the softening that is typical for TPU. It was noted, that the forces required for strain decrease significantly with each strain cycle, and with the five cycles the substrate starts to reach an equilibrium state. Based on this, pre-stretching of the substrate before printing should be experimented in the future. In addition, the plastic deformation of the interconnects was reviewed. After the first cycle, the average residual strain was approximately 11.3% and after the fifth cycle it was 15.2%. It was also noticed, that this residual strain partly diminishes, which is typical behavior for TPU substrate. On average, one minute after the first cycle the residual strain had decreased to 8.6% and after the fifth cycle the corresponding strain was 12.4%. These mechanical properties of the TPU substrate should also be reviewed in the future if they have effect on the electrical performance of the interconnects. In the mechanical tests, it was also discovered, that the Poisson Ratio for the samples is $v = 0.7$.

Last, a demonstration circuit was made with the stretchable traces on a textile. In the demonstration circuit, the strain test pattern made from TPU and ECM CI-1036 ink is heat laminated on the textile. The trace of the pattern is cut from one point, and an LED is attached to the circuit to demonstrate the initial performance of the textile-integrated circuit. This demonstration was successful, as the textile-integrated LED-circuit implemented by using stretchable electronics materials worked correctly.

For future work, it is proposed that the thicknesses and line widths should be measured with a higher precision. This could be done for example with AFM or interferometry. This will give more understanding about the deviations in the initial electrical properties of the samples. In addition, this might help to decrease the sheet resistances to the values lower than 10.0 $m\Omega/\square$, which is stated on the ink's datasheet. One possibility for this difference is that the resulting line thicknesses are lower than 8 µm, which is the specified dry film thickness in the datasheet of the ink. In addition, the deviations in the manufacturing processes should be reduced. This could be done by investigating the differences between the behaviors of the operators, or using a printer with more precise control over the printing parameters. More strain tests should be done with different parameters. The effects of different stretch rates should be reviewed, and based on this data cyclic testing should be done to further understand the durability of the manufactured interconnects. In addition, different substrate and ink combinations should be ex-

perimented. The textile-integrations should be also further experimented, and the electrical and mechanical properties of the textile-integrated printed stretchable substrates should be evaluated.

7. REFERENCES

[1] F. a. F. Marques, D. M. D. Ribeiro, M. F. M. Colunas, and J. P. S. Cunha, A real time, wearable ECG and blood pressure monitoring system, *6th Iber. Conf. Inf. Syst. Technol. (CISTI 2011)*, pp. 1–4, 2011.

[2] G. Yang, L. Xie, M. Mantysalo, X. Zhou, Z. Pang, L. Xu, S. Kao-Walter, Q. Chen, and L. Zheng, A Health-IoT Platform Based on the Integration of Intelligent Packaging, Unobtrusive Bio-Sensor and Intelligent Medicine Box, *IEEE Trans. Ind. Informatics*, vol. PP, no. 99, pp. 1–1, 2014.

[3] Y. L. Zheng, X. R. Ding, C. C. Y. Poon, B. P. L. Lo, H. Zhang, X. L. Zhou, G. Z. Yang, N. Zhao, and Y. T. Zhang, Unobtrusive sensing and wearable devices for health informatics, *IEEE Trans. Biomed. Eng.*, vol. 61, no. 5, pp. 1538–1554, 2014.

[4] T. Someya, *Stretchable Electronics*. Wiley-VCH, 2013.

[5] K. Tehrani, M. Andrew, Introduction to Wearable Technology What is Wearable Technology? What are Wearable Devices?, Wearable Devices, 2014. [Online] Available: http://www.wearabledevices.com/what-is-a-wearable-device/ [Accessed on: 14.10.2015].

[6] A. Rund, Wearable Technologies - Has the Next Enterprise Game Changer Arrived?, Frost & Sullivan, 2014. [Online] Available: http://www.marketresearch.com/product/sample-8599138.pdf [Accessed on: 20.10.2015]

[7] S. Cirani and M. Picone, Computing for the Internet of Things, pp. 35–41, 2015.

[8] C. Tudor-Locke, *Manpo-Kei: The Art and Science of Step Counting*. 2003.

[9] E. R. Burke, *Precision Heart Rate Training*. Human Kinetics, 1998.

[10] T. S. Perry, A Temporary Tattoo That Senses Through Your Skin, *IEEE Spectrum*, pp. 26–31, 2015.

[11] J. Zieba, M. Frydrysiak, L. Tesiorowski, and M. Tokarska, Textronic clothing to ECG measurement, *MeMeA 2011 - 2011 IEEE Int. Symp. Med. Meas. Appl. Proc.*, pp. 2–6, 2011.

[12] B. Huyghe, H. Rogier, J. Vanfleteren, and F. Axisa, Design and manufacturing of stretchable high-frequency interconnects, *IEEE Trans. Adv. Packag.*, vol. 31, no. 4, pp. 802–808, 2008.

[13] S. R. Forrest, The path to ubiquitous and low-cost organic electronic appliances on plastic., *Nature*, vol. 428, no. 6986, pp. 911–918, 2004.

[14] D. Roylance, Mechanics of Materials, Introduction to Elastic Response, MIT OpenCourseWare, 1999. [Online] Available: http://ocw.mit.edu/courses/materials-science-and-engineering/3-11-mechanics-of-materials-fall-1999/index.htm [Accessed on: 28.07.2015].

[15] Engineering Stress-strain Curve: Part One, Total Materia, 2001. [Online] Available: http://www.totalmateria.com/page.aspx?ID=CheckArticle&site=kts&LN=EN&NM=43 [Accessed on: 14.10.2015].

[16] D. Roylance, Mechanics of Materials, Stress-Strain Curves, MIT OpenCourseWare, 2001. [Online] Available: http://ocw.mit.edu/courses/materials-science-and-engineering/3-11-mechanics-of-materials-fall-1999/ [Accessed on: 29.07.2015].

[17] Technical Data PLATILON ® U Highly Elastic Polyurethane Films, Germany, Epurex Films GmbH & Co. KG. Feb. 2012. [Online] Available: https://www.films.bayer.com/en/Products/~/media/013045757CC2401D83DF0B6F1169CAB5.ashx?la=en&force=1 [Accessed on: 29.07.2015].

[18] H. J. Qi and M. C. Boyce, Stress-Strain Behavior of Thermoplastic Polyurethane, Mechanics of Materials, vol. 37, no. 8, pp. 817–914, 2005.

[19] D. H. Kim, J. Xiao, J. Song, Y. Huang, and J. a. Rogers, Stretchable, curvilinear electronics based on inorganic materials, *Adv. Mater.*, vol. 22, no. 19, pp. 2108–2124, 2010.

[20] K. S. Kim, K. H. Jung, and S. B. Jung, Design and fabrication of screen-printed silver circuits for stretchable electronics, *Microelectron. Eng.*, vol. 120, pp. 216–220, 2014.

[21] S. Yao and Y. Zhu, Nanomaterial-Enabled Stretchable Conductors: Strategies, Materials and Devices, *Adv. Mater.*, 2015.

[22] CI-1036, Highly Conductive & Highly Flexible Silver Ink, Technical Data Sheet, ECM Technical Data Sheet, 2010. [Online] Available: http://www.conductives.com/pdfs/CI-1036.pdf [Accessed on: 07.08.2015].

[23] ECM, CI-1036 Safety Datasheet.

[24] T. Liimatta, E. Halonen, H. Sillanpää, J. Niittynen, and M. Mäntysalo, Inkjet Printing in Manufacturing of Stretchable Interconnects, IEEE Conference Publications, 2014.

[25] A. Hobby, Printing Thick Film Hybrids, DEK Printing Machines Ltd., 1997. [Online] Available: http://www.gwent.org/gem_thick_film.html [Accessed on: 10.08.2015].

[26] SCF-300, 550 - SCF Series Screen Printer - Instruction Manual. Eickmeyer GmbH.

[27] S. Enderling, C. L. Brown, S. Smith, M. H. Dicks, J. T. M. Stevenson, M. Mitkova, and M. N. Kozicki, Sheet resistance measurement of non-standard cleanroom materials using suspended Greek cross test structures, *IEEE Trans. Semicond. Manuf.*, vol. 19, no. 1, pp. 2–9, 2006.

[28] T. Liimatta, Inkjet Printing in Manufacturing of Stretchable Interconnects, 2014.

[29] The Anderson-Darling statistic, Minitab 17 Support, 2015. [Online] Available: http://support.minitab.com/en-us/minitab/17/topic-library/basic-statistics-and-graphs/introductory-concepts/data-concepts/anderson-darling/ [Accessed on: 05.10.2015].

[30] Why should I use a 2-sample t test?, Minitab 17 Support, 2015. [Online] Available: http://support.minitab.com/en-us/minitab/17/topic-library/basic-statistics-and-graphs/hypothesis-tests/tests-of-means/why-use-2-sample-t/ [Accessed on: 05.10.2015].

[31] C. J. Chieh, Making Sense of the Two-Sample T-Test, iSixSigma. [Online] Available: http://www.isixsigma.com/tools-templates/hypothesis-testing/making-sense-two-sample-t-test/ [Accessed on: 05.10.2015].